INFORMATION TO USERS

RICE UNIVERSITY

Dynamical Analysis and Control of Longitudinal Electromagnetic Levitation

by
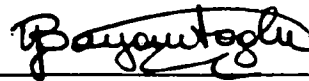
Remzi Artar

A THESIS SUBMITTED
IN PARTIAL FULFILLMENT OF THE
REQUIREMENTS FOR THE DEGREE

Master of Science

APPROVED, THESIS COMMITTEE:

Dr. Fathi H. Ghorbel, Chairman
Associate Professor
Mechanical Engineering & Materials
Science

Dr. Yildiz Bayazitoglu,
Harry S. Cameron Professor
Mechanical Engineering & Materials
Science

Dr. John E. Akin,
Professor
Mechanical Engineering & Materials
Science

Dr. James B. Dabney,
Assistant Professor
System Engineering
University of Houston-Clear Lake

Houston, Texas

August, 2001

UMI®

Dynamical Analysis and Control of Longitudinal Electromagnetic Levitation

Remzi Artar

Abstract

Electromagnetic levitation is a unique technique both for measurements of the thermophysical properties of metals and for producing homogeneous melt in material processing. To maintain stability of the levitated sample is one of the most notable difficulties observed in this technique. The longitudinal levitator developed by Bayazitoglu and Shampine overcomes most of the drawbacks that are inherent in currently used levitator and can support more massive samples than those that can be supported by existing devices. On the other hand, the undesired sample oscillations have been experienced unless the sample is released very near its equilibrium position as levitation is begun. 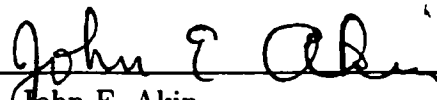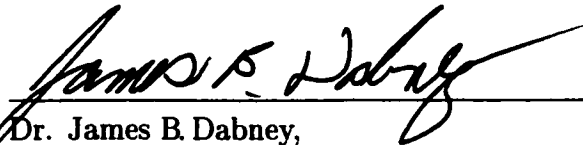To approach this problem, a dynamical model of the process is needed. This study addresses dynamical analysis and control of the longitudinal electromagnetic levitation. The levitation force is analytically derived considering the effect of the sample's motion. Based on the dynamical analysis, a nonlinear dynamical model of the process is derived. Using the numerical solution of the dynamical model, the influences of the system parameters on the dynamical behavior of the sample are illustrated. To achieve stable levitation the derived dynamical model has been linearized and implementing a linear control technique, the sample's undesired oscillations have been succesfully eliminated at very begining of the levitation.

Acknowledgments

I would like to thank my advisor, Dr. Fathi Ghorbel for his guidance and support during my graduate study. I would like to thank Dr. Yildiz Bayazitoglu and Dr. Jim Dabney for their valuable support and Dr. John E. Akin for being in my thesis committee.

I would also like to express my gratitude to my colleagues: Kun Lu, Serkan Gugercin, Athanasios Athanasiades, Oguzhan Guven, Gokturk Tunc, and Kaan Ozturk for the friendship they offered to me.

Finally, I would like to thank my wife and my parents for their support and encouragement in my endeavor.

Table of Contents

List of Figures

Chapter 1

Introduction

As one of the emerging megatechnologies, advanced materials technology requires completely understood fundamental theories in order to meet the new demands and new standards arising in the first decade of the twenty-first century. To improve our theoretical and experimental capabilities to analyze the fundamental structure of metals, their thermophysical properties must be accuretely and precisely measured. Electromagnetic levitation is a unique technique, which provides very accurate results for these measurements, eliminating the interaction between metal sample and the container. The technique is also used to produce a very pure and homogeneous melt in materials processing.

1.1 Electromagnetic Levitation

Electromagnetic levitation is a well-known technique of containerless processing. When a electrically conducting sample is placed in an alternating magnetic filed, the induced eddy currents generate firstly a levitation force, which can support the sample against gravity, and secondly a resistive heating, which can melt it.

Electromagnetic levitation systems consist of three parts: A High Voltage DC Power Supply, an Oscillator Circuit, and a Levitator.

1)*High Voltage DC Power Supply:* It amplifies and rectifies the line voltage to supply a high DC voltage to the oscillator circuit.

2)*Oscillator Circuit:* This unit converts the high DC voltage to radio frequency power

(RF Power), which is applied to the levitator.

3)*Levitator:* It generates an alternating magnetic field using the RF power.

The alternating magnetic field creates two major effects on the sample: heating and levitation force.

Heating: The alternating magnetic field excites eddy currents to flow within a sample placed in the field. The eddy currents cause heating due to the resistivity of the metal sample.

Levitation Force: The eddy currents also generate a force called Lorentz Force, which can support the sample against gravity. The design of the levitator affects both the amount of the heat generated and the magnitude of the levitation force.

1.2 Applications

Electromagnetic levitation is commonly used to produce a very pure and homogeneous melt in materials processing. In recent years, the melting technique, a well-known application of material processing, has become very important in improving the quality of metal and in developing new alloys. In the conventional melting method, contamination usually takes place between the molten metal and the crucible. The use of electromagnetic levitation is considered to be one of the most appropriate methods for this problem [1, 13, 27].

Aside from its advantages in the melting process, electromagnetic levitation also has been found to be useful in the determination of the thermophysical properties of metals [1, 2, 6, 8, 26, 33]. The measurements of the thermophysical properties of solids and liquids at high temperatures are always influenced by their containers. Electromagnetic levitation technique eliminates the interaction between metal samples and the container and provides very accurate results for these measurements.

Thermophysical property measurements by electromagnetic levitation technique include surface tension measurements [5, 12, 28, 34] liquid metal density measurements [8, 31], optical property measurements[21, 22], liquid metal viscosity measurements [8], and electrical conductivity measurements [29].

1.3 Motivation

Since *Okress et al.* [11] demonstrated the levitation technique in 1952, different aspects of this technique have been analyzed. Most of the literature on levitation has been concerned with calculations of the forces on a conducting body [15, 24, 33];and experimental studies[11, 15, 24].

Rony [30] calculated the force on a conducting sphere when it is placed in a uniform z-directed alternating magnetic field. Fromm and Jehn [15] studied the forces on the metal samples when they were placed in the field produced by circular current carrying loops and compared the results with experimental data. Li [23] analyzed the electromagnetic and thermal phenomena in a magnetically-levitated metallic sphere. Several papers [11, 24, 33] gave detailed reports on levitation experiments with different metals using various coils.

The most notable difficulty observed in this technique is maintaining stability of the levitated sample inside the levitator, as reported in [2, 8, 25]. However, most of the methods developed to measure thermophysical properties by using levitation technique require stable levitation as a condition [2, 8, 25, 28]. For instance, in high temperature density measurements of metals, maintenance of sample stability is of primary importance, since an accurate measurement largely depends on the quality of the photographs taken during the process. Unexpected vibration and oscillations of the sample have to be avoided in order to obtain clear and symmetrical profiles.

Okress [11] made the first quantitative calculations on the levitation force and gave an approximate formula for the levitation force exerted on a homogeneous metal sphere in the electromagnetic field produced by a single loop or two equal coaxial loops. However, he indicated the necessity of investigating the magnetic field distribution for stable leviation of molten as well as solid metals.

Baykara *et al* [8]reviewed containerless thermophysical property measurements and reported that violent rotation, vibration and other uncontrollable instabilities can cause problems during the high temperature density measurements process.

Przyborowski *et al* [28] studied the surface tension measurement of molten silicon by using electromagnetic levitation, but he also reported that the sample instability was the one of the main sources of temperature measurement errors.

Krishnan [21] studied shape oscillations observed in electromagneticaly levitated liquid metal droplets in order to determine the surface tension of the metal at high temperatures. Although his results were in reasonable agreement with the works of others, considering the sustained oscillations which could not be easily explained with currently available models, he indicated the necessity of analytical and numerical work to model the interaction of electromagnetic fields with regard to oscillations effects.

Recently, Bayazitoglu and Shampine [3] introduced a longitudinal levitator which has some unique advantages, such as good visual access to the sample, the ability to support more than one sample, and the ability to minimize the tendency of the sample to rotate and vibrate. On the other hand, the authors reported that the sample must be released at its equilibrium position as levitation is begun, otherwise substantial sample vibrations are experienced. In brief, the chief diffuculty with the electromagnetic levitation is to obtain a stable motion of the sample.

Several approaches have been proposed for stable levitation in the literature [9, 14, 17, 25, 37]. Bocian and Young [14] considered solid-state stability of a lev-

itating sample by using a circuit equivalent model of the excitation coil in conical levitator, and studied the possibilities for vertical stability in terms of levitation force predicted from electromagnetic theory. Holmes [17] studied the levitation force on metal samples in conical levitators and derived a criterion for stability of the sample based on the coil geometry. However, neither of these works considered the effect of the sample's motion in the calculations.

In [9], an experimental apparatus was suggested to allow stable levitation of a melted paramagnetic body applying combination of static magnetic and electromagnetic forces. Unfortunately, the technique was applicable only for the levitation of a paramagnetic conducting material (iron-silicon alloy).

A few researchers have attempted to solve the stability problem using a closed loop control strategy. Yoda *et al.* [37] designed a device (U.S. Patent 5155651)with a position sensor to control the rotation of the sample for conical levitators. The levitator had a position detector for detecting the position of a sample. The detector also controled the output voltage of the variable power, which connects to a pair of planar electrodes.

In addition, Minegawa *et al.* [25] applied a closed loop control technique to eliminate the oscillations at the transition from normal gravity to microgravity in a conical levitator. They used three pairs of search coils and two CCD cameras to measure the position of the levitated sample. Using these data and applying curve fitting analysis, they obtained an approximate model of the motion of the sample. Based on this model, they designed a PID (proportional, integral, and differential) control law to control the electromagnetic power for a stable levitation.

Although these several strategies have been proposed for stable levitation in conical levitators, no one has attempted to analyze the instability problem for the longitudinal levitator. Since Bayazitoglu and Shampine [3] introduced the longitudinal

levitator in 1996, different aspects of this levitator have been analyzed. Shampine and Bayazitoglu [32, 33] were concerned with the calculations of the lifting force on a cylindrical sample and conducted some expmerimental studies. He also explained the vertical stability conditions in the longitudinal levitator assuming stable levitation. Nonetheless he did not study the effect of initial position of the sample on the vertical stability through a dynamical model of the levitated sample. This effect is analyzed in this work for the first time and the results are given in Chapter 4.

Bayazitoglu and Zhong [38, 39] further examined the concept by developing general analytical expressions for the lifting force and the heat generation in cylindrical samples supported by n-pole longitudinal levitators. They also studied the determination of transient temperature, which is of fundamental importance in material processing. But they found that the initial position (if not the equilibrium) of the sample excited substantial sample vibrations, which caused considerable differences between the theoretical and experimental results of the transient temperature measurements.

Recently, Bayazitoglu and Young [7] studied 2-pole longitudinal levitator for use in containerless manufacturing. They reported the vertical oscillations of the sample as the practical obstacles for the longitudinal levitation process.

These drawbacks of the longitudinal levitation process imply a need for the dynamical model of the levitated sample, both to explain the dynamics of the reported sample's oscillations and to design an appropriate control strategy for a stable levitation. In addition, considering its remarkable superiority (mentioned above), stability achieved through dynamical modeling might enable longitudinal levitation to become a containerless manufacturing process.

In response to these requirements, described above, this study derived a dynamical model of the levitated metal sample in longitudinal levitator. The study analyzed the

solid-state phase, considering the effect of the sample's motion inside the levitator. The main objectives and contributions of this work can be summarized as follows:

- This work describes for the first time the dynamical model of the levitated sample in the longitudinal levitator.

- One of the main contributions of this work was to characterize the levitation force considering the effect of the sample's motion. This characterization included an analytical derivation of the damping component of the levitation force for the first time. Previous works (mentioned above) derived the levitation force assuming the sample is stationary in the levitator.

- This study's analysis showed that the sample's motion in the levitator produces a non-linear damping effect, which is a function of the system parameters such as the coil current, current frequency, coil configuration and the sample's diameter.

- To provide a framework for further investigation of the levitation process, the influences of the system parameters on both the lifting and damping components of the levitation force were separately analyzed.

- The results of the dynamical analysis were succesfully utilized to create a numerical simulation model in MATLAB to produce the position, the velocity and the lifting force trajectories for the first time.

- Several simulations were performed to illustrate the effect of the initial position, damping force, coil current, and coil configuration on the sample's dynamic behavior. The simulation results not only verify the earlier observations but also depict the dynamics of the sample's reported substantial oscillations.

- Implementing two feedback control techniques, the PD based and the pole-placement, a stable levitation was achieved eliminating the sample oscillations at very beginning of the levitation.

The drawbacks of the currently used levitators and the superiority of the longitudinal levitators are discussed in Chapter 2. The components of the electromagnetic field in the longitudinal levitator are obtained by using the fundamental laws of electromagnetic theory.

In Chapter 3, the Lorentz Force Field is characterized considering the motion of the sample in the vertical plane. This characterization includes an analytical derivation of the damping component of the levitation force. The influences of the system parameters such as the coil current, current frequency, coil configuration and the sample's diameter on both the lifting and damping components of the levitation force are analyzed.

In Chapter 4, to depict the dynamics of the levitated sample and to verify the earlier observations of the substantial sample's oscillations, the dynamical model of the sample is derived considering both the lifting and damping components of the levitation force. The derived model is transformed into state-space form. Using a numerical integration method, the position, the velocity and the lifting force trajectories are produced. In addition, to achieve stable levitation two feedback control techniques, the PD based and the pole-placement, are implemented and the effectiveness of these techniques are verified with several simulations.

Chapter 5 presents the conclusions.

Chapter 2

Electromagnetic Field Analysis

2.1   Longitudinal Electromagnetic Levitator

The currently used levitators, illustrated in Figure 1, suffer from several drawbacks inherent in their designs as mentioned in [3, 32].

-*Limited Sample Shapes:* The coils and the sample pose a degree of axisymmetry about the coil axis, which restricts the kinds of samples that can be levitated. Therefore, samples with large aspect ratios such as cylinders cannot be levitated in currently available levitators.

-*Poor Visual Access:* When these levitators are used as diagnostic instruments to measure the thermophysical properties, they suffer from the problem of sample visibility. The coil design obtructs the view of the sample and makes data collection difficult.

-*Magnetic Hole:* In the currently used levitators, the magnetic pressure on the sample surface vanishes at the top and bottom points. The molten metal is prevented from leaking out of the 'magnetic hole' at the lowest point by surface tension. Therefore there is an upper limit on the mass that can be levitated and melted without 'leakage' in this kind of levitator [14]

-*Position Control of the Sample:* Existing levitators are essentially static devices, that is, they allow very little manipulation of the sample.

-*Poor Lifting Capacity:* Currently used levitators cannot support large samples.

These drawbacks imply a need for a device that can be used to levitate large samples and control them during the levitation process. Recently, Bayazitoglu and Shampine [3] introduced the longitudinal levitators that alleviate most of the problems suffered by the currently used levitators.

Figure 2.1: The Conical Levitator [10]

The longitudinal levitator introduced by Bayazitoglu and Shampine overcomes most of the above drawbacks [3, 32, 33]. It consists of a set of parallel conductors that are formed by bending copper tubing, with neighboring conductors passing current in opposite directions. The coils are made with 6.3 mm and 4.7 mm in diameter copper tubing, through which cooling water is passed. The cooling water is provided to

prevent the coils from overheating due to high current they carry. Figure 2 illustrates an 8-poles longitudinal levitator.

Longitudinal levitator is able to exceed the lifting capacity of the conventional levitators by increasing the volume of the sample without increasing its weight. The volume increase is made possible by increasing the length and the width of the sample. The longitudinal levitator is capable of supporting spherical and non-spherical sample shapes, such as cylinders and rectangular blocks, and has very good visual access to the sample. In addition, it can support comparatively large sample weight while avoiding excessive heating rates, thus overcoming the problem of the 'magnetic hole' [3].

Because of these advantages, the longitudinal levitator has potential for becoming a 'containerless' manufacturing process. Bayazitoglu and Shampine built and tested different configurations of the longitudinal levitators with cross sections as shown in Figure 2.3. Considering its remarkable superiority, this study addresses the dynamical analysis and control of the longitudinal levitation process.
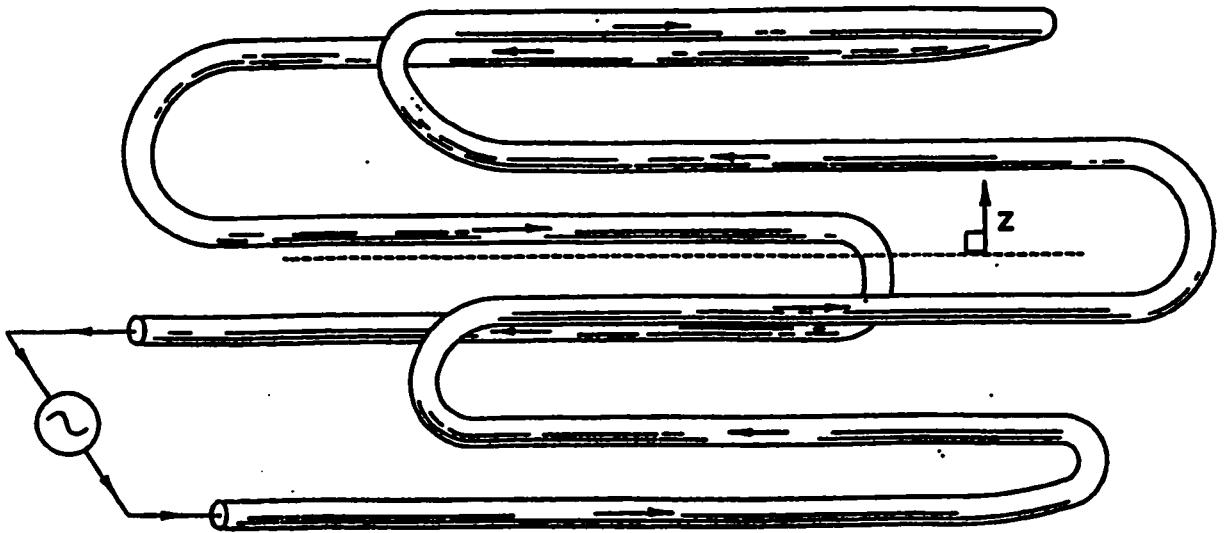
Figure 2.2: The Longitudinal Levitator developed by Bayazitoglu and Shampine [4]
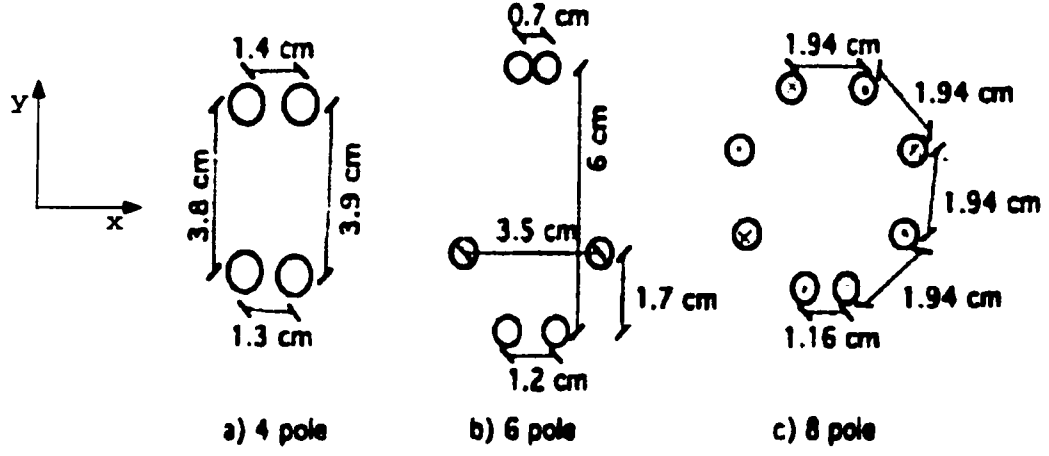
Figure 2.3: Different configurations of longitudinal levitator. Levitators are reflection symmetric in y-direction and the coordinator center is located in the vertical direction (reproduced from [3])

2.2 Field Analysis

To characterize the levitation force on the sample we need to study the electromagnetic field in the levitator. Shampine and Bayazitoglu [32] analyzed the electromagnetic field of a longitidunal levitator, producing the magnetic flux density and the electric intensity vectors, which will be used in this study. To derive these quantities, a similar procedure given in [32] is followed. The analysis procedes by consideration of a homogeneous cylindrical body with constant permittivity ϵ, permeability μ, and conductivity σ, surrounded by a nonconducting medium characterized by the free-space permittivity ϵ_o, and permeability μ_o. The fundemantal laws of electromagnetic theory, which apply both to the body and the surrounding medium, are given by Maxwell's equations:

$$\nabla \times \mathbf{E} = -\frac{\partial \mathbf{B}}{\partial t}, \tag{2.1}$$

$$\nabla \times \mathbf{B} = \mu(\mathbf{J} + \epsilon \frac{\partial \mathbf{E}}{\partial t}), \tag{2.2}$$

$$\nabla.\mathbf{B} = 0, \tag{2.3}$$

$$\mathbf{J} = \sigma \mathbf{E}. \tag{2.4}$$

where $\mathbf{J}$ is the current density, $\mathbf{B}$ is the magnetic flux density, and $\mathbf{E}$ is the electric intensity. In order to solve these equations, it is useful to define a vector potential, $\mathbf{A}$ such that,

$$\nabla \times \mathbf{A} = \mathbf{B}, \tag{2.5}$$

$$\nabla.\mathbf{A} = 0, \tag{2.6}$$

$$\mathbf{E} = -\frac{\partial \mathbf{A}}{\partial t}, \tag{2.7}$$

where it is assumed that $\nabla.V = 0$. Substituting $\mathbf{A}$ from Equation (2.5), and $\mathbf{E}$ from Equation (2.7), and $\mathbf{J}$ from Equation (2.4) into Equation (2.2) yields

$$\nabla \times (\nabla \times \mathbf{A}) = -\mu\sigma\frac{\partial \mathbf{A}}{\partial t} - \mu\epsilon\frac{\partial^2 \mathbf{A}}{\partial t^2} \tag{2.8}$$

The Laplacian of $\mathbf{A}$ obeys the vector identity given by

$$\nabla^2 \mathbf{A} = \nabla(\nabla \mathbf{A}) - \nabla \times (\nabla \times \mathbf{A}) \tag{2.9}$$

From the definition of A, $\nabla.\mathbf{A} = 0$; hence, Equation (2.9) can be written as

$$\nabla^2 \mathbf{A} - \sigma\mu\frac{\partial \mathbf{A}}{\partial t} - \mu\epsilon\frac{\partial^2 \mathbf{A}}{\partial t^2} = 0 \tag{2.10}$$

If we assume that the time dependence is sinusoidal, $\mathbf{A}$ can be written in the form of phasor notation as

$$\mathbf{A} = Ae^{j\omega t} \tag{2.11}$$

Then the conversion of the time derivative to phasor notation is

$$\frac{\partial \mathbf{A}}{\partial t} \leftrightarrow j\omega \mathbf{A} \tag{2.12}$$

Hence, the governing equation is obtained as in [32]

$$\nabla^2 \mathbf{A} - \sigma\mu j\omega \mathbf{A} + \mu\epsilon\omega^2 \mathbf{A} = 0 \tag{2.13}$$

There are two types of boundary conditions in the system. One of them is the distance, δ, called the skin depth of the medium, which characterizes how well an electromagnetic wave can penetrate into a conducting medium. It is given by the formula [32],

$$\delta = (\frac{1}{2}f\mu\sigma)^{-\frac{1}{2}} \tag{2.14}$$

where f is the frequency. The skin depth is also defined as the depth below the surface of a conductor at which the current density or magnetic field has decreased to $1/e$ at the surface.

The other boundary condition is related to the surface current, which flows on two dielectric media. The tangential component of the magnetic flux density has a discontinuity equal to [32]

$$\vec{n} \times (\Delta B_{tan}) = \mu J_s \tag{2.15}$$

where $\vec{n}$ is the unit vector normal.

2.2.1 The Components of the Electromagnetic Field

Let the X axis be horizontal and let the origin of polar coordinates be the center of the cross-section of the cylinder. Figure 2.1 shows the coordinate system [39]. Where

a is the sample radius and c_m and w are the positions of the coils and the sample, respectively, b_m is the distance between the center of the cylinder and the coil. Since the frequency of the coil current is very high, the electric current flow is distributed essentially on the surface of the coil by the skin effect.
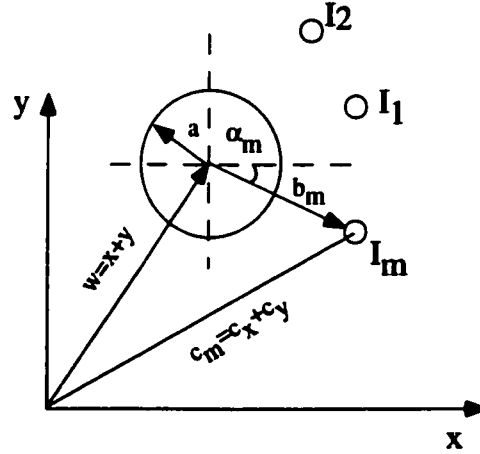
Figure 2.4: The Coordinate System (reproduced from [39])

We suppose that the whole space is divided into three regions, as suggested by Piggott [24]

1) The inside of the cylinder, $r < a$

2) The annular space, $a < r < b$

3) $r > b$

In region 1, only conduction current flows, and Equation (2.13) becomes

$$\frac{1}{r}\frac{\partial}{\partial r}(r\frac{\partial A}{\partial r}) + \frac{1}{r^2}\frac{\partial^2 A}{\partial \theta^2} - j\omega\mu_0\sigma A = 0 \qquad (2.16)$$

A suitable solution is

$$A = \sum_{-\infty}^{\infty} C_n J_n(k_1 r)e^{jn\theta} \qquad (2.17)$$

where $k_1 = \sqrt{-j\omega\mu_0\sigma}$. In region 2, $a < r < b$, Equation (2.13) becomes

$$\frac{1}{r}\frac{\partial}{\partial r}(r\frac{\partial A}{\partial r}) + \frac{1}{r^2}\frac{\partial^2 A}{\partial \theta^2} = 0 \qquad (2.18)$$

In this case, a suitable solution is

$$A = \sum_{-\infty}^{\infty}(D_n r^n - E_n r^{-n})e^{jn\theta} \qquad (2.19)$$

In region 3, there is an additional condition that the field vectors must remain finite at infinity; thus there is no positive of r

$$A = \sum_{1}^{\infty} F_n r^{-n} e^{jn\theta} + \sum_{-\infty}^{0} G_n r^n e^{jn\theta} \qquad (2.20)$$

Applying the second boundary condition (Equation (2.15)) at $r = a$ and $r = b_m$, and also adding in the contributions of the p current filaments, C_n can be obtained as given by [39]

$$C_n = \frac{\frac{\mu_0}{2\pi}\sum_{m=1}^{p}\frac{a^{n-1}}{(c_m - w)^n}\hat{I}_m}{k_1 J_{n-1}(k_1 a)} \qquad (2.21)$$

$$C_{-n} = \frac{\frac{\mu_0}{2\pi}(-1)^n \sum_{m=1}^{p}\frac{a^{n-1}}{(c_m^* - w^*)^n}\hat{I}_m}{k_1 J_{n-1}(k_1 a)} \qquad (2.22)$$

where $\hat{I}_m$ is the coil current of the mth coil pole and the * superscript indicates the conjugate of a complex variable. Finally, the components of the magnetic flux density can be derived similar to Shampine [32]

$$B_r = Re[\sum_{n=-\infty}^{\infty}(\frac{jn}{r})C_n J_n(k_1 r)e^{jn\theta}e^{iwt}] \qquad (2.23)$$

$$B_\theta = Re[-k_1 \sum_{n=-\infty}^{\infty} C_n \acute{J}_n(k_1 r)e^{jn\theta}e^{iwt}] \qquad (2.24)$$

and the amplitude of the z component of electric intensity is

$$E_z = Re[-(\frac{k_1^2}{\mu_0\sigma}) \sum_{n=-\infty}^{\infty} C_n J_n(k_1 r)e^{jn\theta}e^{iwt}] \qquad (2.25)$$

where $\acute{J}_n(k_1 r)$ is the derivative of $J_n(k_1 r)$ with respect to $k_1 r$. As n becomes very large, the series in Equation (2.23), (2.24), and (2.25) are convergent for all physically possible values of the position of the sample. The details of the derivation can be found in [32, 33, 39].

Having derived these equations, we can start to analyze the levitation force, which will be used in the dynamical analysis.

Chapter 3

Force Analysis

3.1 Lorentz Force Field

If a metallic specimen moves along the vertical axis, Equation (2.1)(Faraday's law) should be reconsidered and one more term should be added to the right side of the equation. Let us write the Faraday's law for a moving medium [35],

$$\nabla \times \hat{\mathbf{E}} = -\nabla \times \left(\frac{\partial \mathbf{A}}{\partial t}\right) + \nabla \times (\mathbf{v} \times \mathbf{B}) \qquad (3.1)$$

where $\hat{\mathbf{E}}$ is the total electric intensity, and $\mathbf{v}$ is the velocity vector of the sample. Grouping the terms gives

$$\nabla \times \left(\hat{\mathbf{E}} + \left(\frac{\partial \mathbf{A}}{\partial t}\right) - (\mathbf{v} \times \mathbf{B})\right) = 0 \qquad (3.2)$$

and finally,

$$\hat{\mathbf{E}} = -\frac{\partial \mathbf{A}}{\partial t} + \mathbf{v} \times \mathbf{B} - \nabla V \qquad (3.3)$$

where V is the electric potential. Since there is no imposed current in the metallic specimen, the term ∇V is zero. Therefore, considering Equation (2.7), the current density for a moving medium is

$$\mathbf{J} = \sigma(\mathbf{E} + \mathbf{E}') \qquad (3.4)$$

where $\mathbf{E}'$ is the velocity dependent electric intensity, which is given by

$$\mathbf{E}' = \mathbf{v} \times \mathbf{B} \qquad (3.5)$$

The net Lorentz force on the cylinder sample is the integral of the cross product of the current density and the magnetic flux density. In calculating the total levitation force, it is convenient to use complex coordinates, where a point in the Cartesian plane is represented by $x + jy$. Thus, the total levitation force per unit length is

$$\mathbf{F} = Re \int_0^{2\pi} \int_0^a \mathbf{J} \times \mathbf{B} r dr d\theta \tag{3.6}$$

Substituting Equation (3.4) into Equation (3.6)

$$\mathbf{F} = Re \int_0^{2\pi} \int_0^a \sigma \mathbf{E} \times \mathbf{B} r dr d\theta + Re \int_0^{2\pi} \int_0^a \sigma \mathbf{E}' \times \mathbf{B} r dr d\theta \tag{3.7}$$

Let the first and the second term of the equation be the levitation and the damping component of the levitation force, respectively. Thus,

$$\mathbf{F}_l = Re \int_0^{2\pi} \int_0^a \sigma \mathbf{E} \times \mathbf{B} r dr d\theta \tag{3.8}$$

and

$$\mathbf{F}_d = Re \int_0^{2\pi} \int_0^a \sigma (\mathbf{v} \times \mathbf{B}) \times \mathbf{B} r dr d\theta \tag{3.9}$$

The reason F_d is called the damping component of the levitation force will be explained later.

3.2 Lifting Force Analysis

3.2.1 Lifting Force

Equation (3.8) represents the lifting component of the levitation force as it was mentioned above. Rewriting $Re(\mathbf{B})$ as $(\mathbf{B} + \mathbf{B}^*)$ as suggested in [39] yields the following,

$$\mathbf{F}_l = \frac{1}{2} Re \int_0^{2\pi} \int_0^a \sigma \mathbf{E} \times \mathbf{B} r dr d\theta + \frac{1}{2} Re \int_0^{2\pi} \int_0^a \sigma \mathbf{E} \times \mathbf{B}^* r dr d\theta \tag{3.10}$$

by defining

$$\mathbf{F}_l^T = \frac{1}{2} Re \int_0^{2\pi} \int_0^a \sigma \mathbf{E} \times \mathbf{B} r dr d\theta \tag{3.11}$$

$$\mathbf{F}_l^A = \frac{1}{2} Re \int_0^{2\pi} \int_0^a \sigma \mathbf{E} \times \mathbf{B}^* r \, dr \, d\theta \tag{3.12}$$

We are interested in $\mathbf{F}_l^A$, which is the time averaged lifting force. Because both $\mathbf{E}$ and $\mathbf{B}$ have a time term $e^{i\omega t}$, the time averaged of $\mathbf{F}_l^T$ is zero.

Expanding $\mathbf{B}$ in the cylindrical coordinates, we can determine the time averaged lifting force:

$$\mathbf{F}_l^A = \frac{1}{2} Re \int_0^{2\pi} \int_0^a \sigma E \mathbf{k} \times (B_r^* \mathbf{e_r} + B_\theta^* \mathbf{e_\theta}) r \, dr \, d\theta \tag{3.13}$$

Defining F_l^{Ax} as the horizontal force in x-direction, and F_l^{Ay} as the vertical force or the lifting force in y-direction,

$$F_l^{Ax} = \frac{1}{2} Re \int_0^{2\pi} \int_0^a \sigma E(B_r^* \sin\theta + B_\theta^* \cos\theta) r \, dr \, d\theta \tag{3.14}$$

$$F_l^{Ay} = \frac{1}{2} Re \int_0^{2\pi} \int_0^a \sigma E(B_r^* \cos\theta - B_\theta^* \sin\theta) r \, dr \, d\theta \tag{3.15}$$

By substituting the electromagnetic levitation field Equations (2.23),(2.24), and (2.25) into the equations above and using Bessel Function's iterative formula, we can obtain

$$F_l^{Ax} = \frac{\pi \mid k_1 \mid^2}{4\mu_0} \sum_{-\infty}^{\infty} Q_n [k_1 C_n (C_{n+1}^* - C_{n-1}^*) + k_1^* C_n^* (C_{n+1} - C_{n-1})] \tag{3.16}$$

$$F_l^{Ay} = \frac{-i\pi \mid k_1 \mid^2}{4\mu_0} \sum_{-\infty}^{\infty} Q_n [k_1 C_n (C_{n+1}^* + C_{n-1}^*) - k_1^* C_n^* (C_{n+1} + C_{n-1})] \tag{3.17}$$

where

$$Q_n = \int_0^a J_n(k_1 r) J_n(k_1^* r) r \, dr \tag{3.18}$$

Defining a complex force,

$$F_l = F_l^{Ax} + i F_l^{Ay} \tag{3.19}$$

and using the results of Equation (3.16) and(3.17), we can write the complex force

$$F_l = \frac{\pi \mid k_1 \mid^2}{2\mu_0} \sum_{-\infty}^{\infty} Q_n [k_1 C_n (C_{n+1}^* - k_1^* C_n^* (C_{n-1}] \tag{3.20}$$

which can also be written as

$$F_l = \frac{\pi \mid k_1 \mid^2}{2\mu_0} k_1 \sum_{-\infty}^{\infty} (Q_n - iQ_{n+1}) C_n C_{n+1}^* \qquad (3.21)$$

Finally, by using the integral formulation for the Bessel functions, we can obtain the time averaged lifting force per unit length as the following, which is the imaginary part of the force formula given by Shampine and Bayazitoglu [32]

$$F_{ly} = Im\{\frac{\mu_0 \hat{I}_m^2}{4\pi a} \sum_{n=1}^{\infty} [\{\sum_{m=1}^{p} (\frac{a}{c_m - iy})^n\}\{\sum_{m=1}^{p} (\frac{a}{c_m^* + iy})^{n+1}\} Re \frac{J_{n+1}(k_1 a)}{J_{n-1}(k_1 a)}]\} \qquad (3.22)$$

Details can be found in Appendix A.

3.2.2 Lifting Force Simulation Results

Using Equation (3.22), it is possible to determine the position of the levitated sample and analyze the lifting capacity of the longitudinal levitator. Equation (3.22) also shows that the lifting force depends on the geometry of the levitator, the coil current, and the current frequency, and the sample's radius and conductivity. In order to analyze the effects of these parameters on the lifting force, a MATLAB code was written for a six-poles asymetric longitudinal levitator (shown in Figure 2.3.b), which is the best trade-off among the other configurations in terms of lifting capacity and the horizontal stability. In this analysis, the coil current is 568 A at a frequency of 292 kHz, which is the value of the actual apparatus at Rice University. The parameters of the sample are given below.

The material of the sample: Aluminum

The diameter of the sample: 10 mm.

The length of the sample: 10 mm.

The density of aluminum: 2700 kg/m^3

The electric conductivity of the sample: 3.57×10^7 Siemens/m

Vertical lifting force versus vertical position along the centerline of the levitator is

shown in Figure 3.1. The negative part of the curve has no positive effect on the lifting force because it is in the same direction as gravity. The positive part of the curve is the actual levitation region. In this region if the levitated sample is influenced by a small disturbance in the vertical direction, it will eventually be restored to the original levitation position by the change in the lifting force magnitude, whether the disturbance is upward or downward. Detailed dynamical analysis of this behaviour will be discussed in the next chapter.

The coil current effect on the lifting force is illustrated in Figure 3.2. At a given frequency, the lifting force depends on the square of the coil current. When the other system parameters such as frequency, coil geometry, and sample radius are fixed, the coil current will determine the levitation position and the lifting capacity of the levitator. In Figure 3.2, the equilibrium points shows the levitation positions of the sample for two different values of the current.

The influence of the diameter of the sample on the lifting force is illustrated in Figure 3.3. From the figure, it can be seen that the lifting force increases as the sample diameter increases.

At low frequencies, the lifting force is proportional to the square root of the frequency. This relationship is shown in Figure 3.4. On the other hand, the lifting force reaches an asymptotic value at high frequency as illustrated in Figure 3.5. Thus, the lifting force becomes independent of the current frequency at sufficiently high frequencies.

At relatively low frequencies, the electrical conductivity of the sample can significantly affect the lifting force. Figure 3.6 shows that the lifting force acting on the sample of copper and aluminum at 5 kHz. From the figure, it can also be seen that the lifting force increases as the electrical conductivity increases. On the other hand,

the effect of the electrical conductivity becomes relatively weak at higher frequencies. Figure 3.7 illustrates the lifting force acting on the same samples at 300kHz.

The influence of the coil configuration is illustrated in Figure 3.8. In the figure, coil 1 is the original levitator, and coil 2 is the modified levitator, which its two poles in the middle were approached 1.2 cm to each other. As can be seen from the figure, the modified levitator produces less lifting force and shrinks the levitation range. The coil configuration can dramatically change the dynamical behaviour of the levitated sample. This effect will be analyzed in chapter 4.
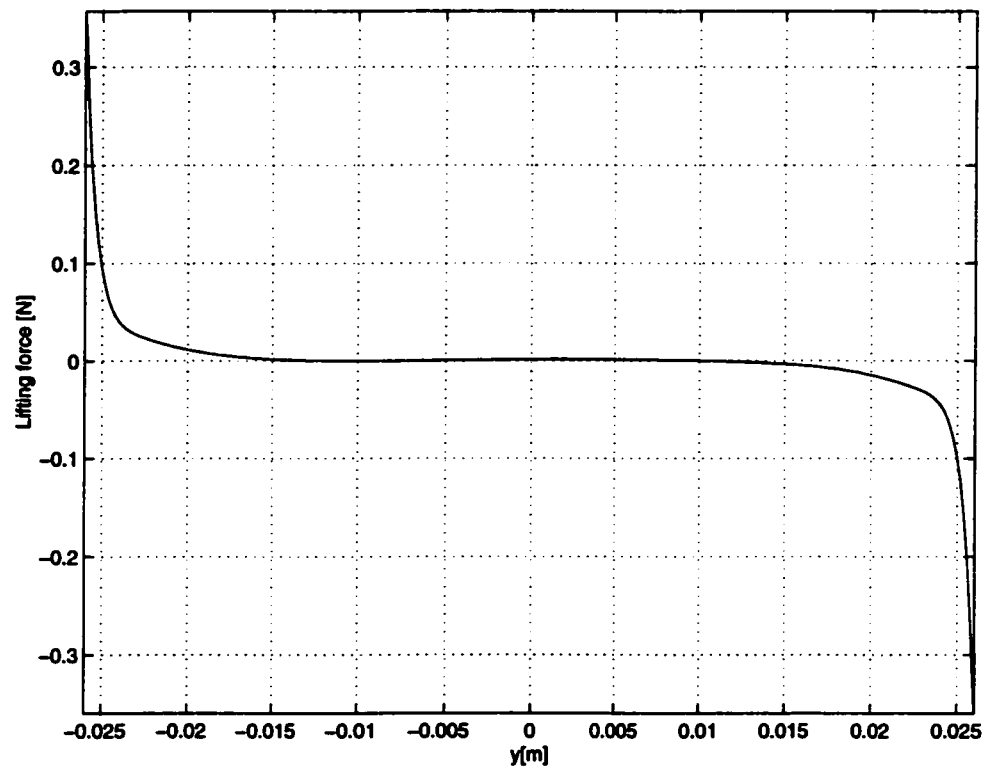
Figure 3.1: Vertical lifting force *versus* vertical position along the centerline of the 6-pole levitator.
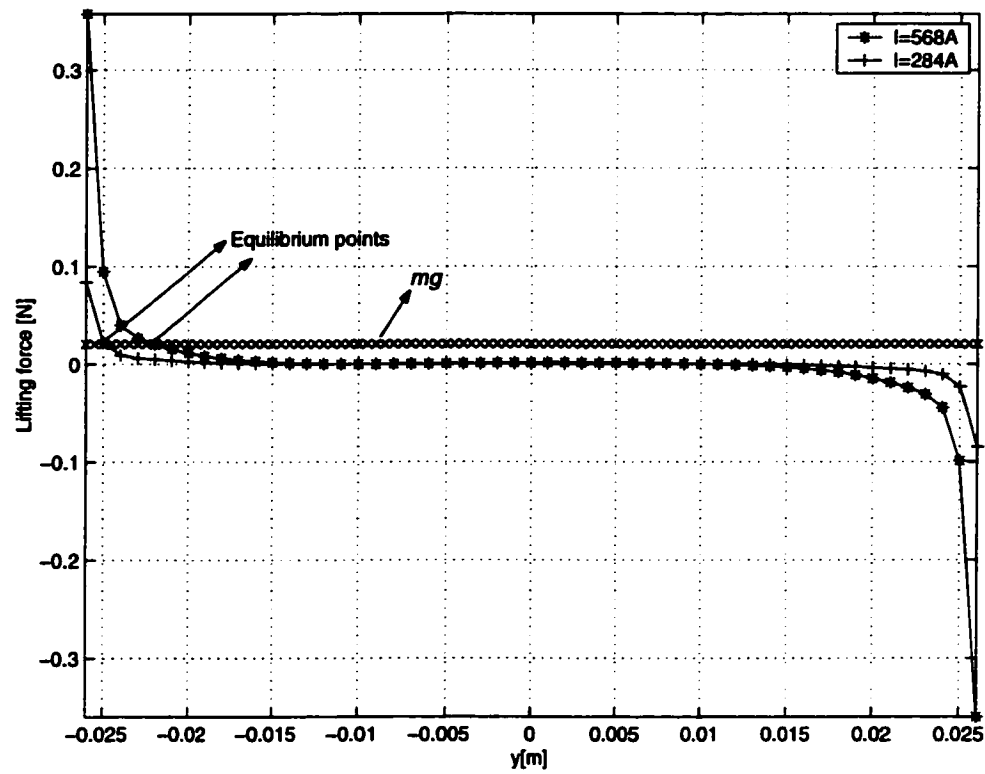
Figure 3.2: The influence of the coil current on the lifting force.
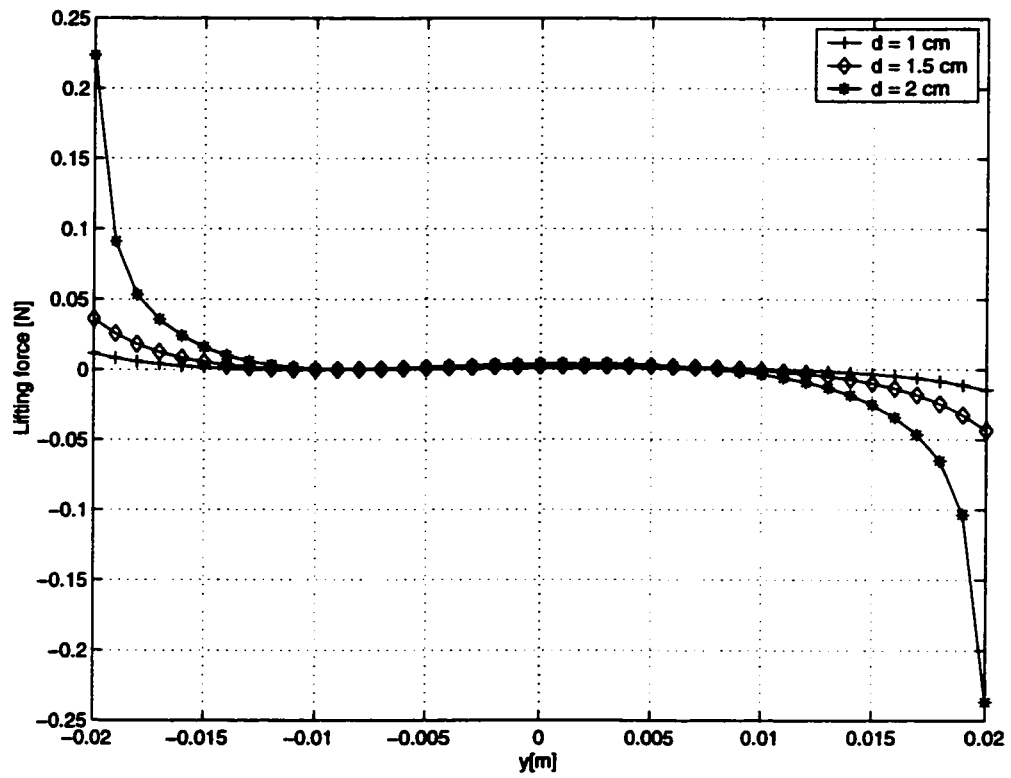
Figure 3.3: The influence of the sample diameter on the lifting force.
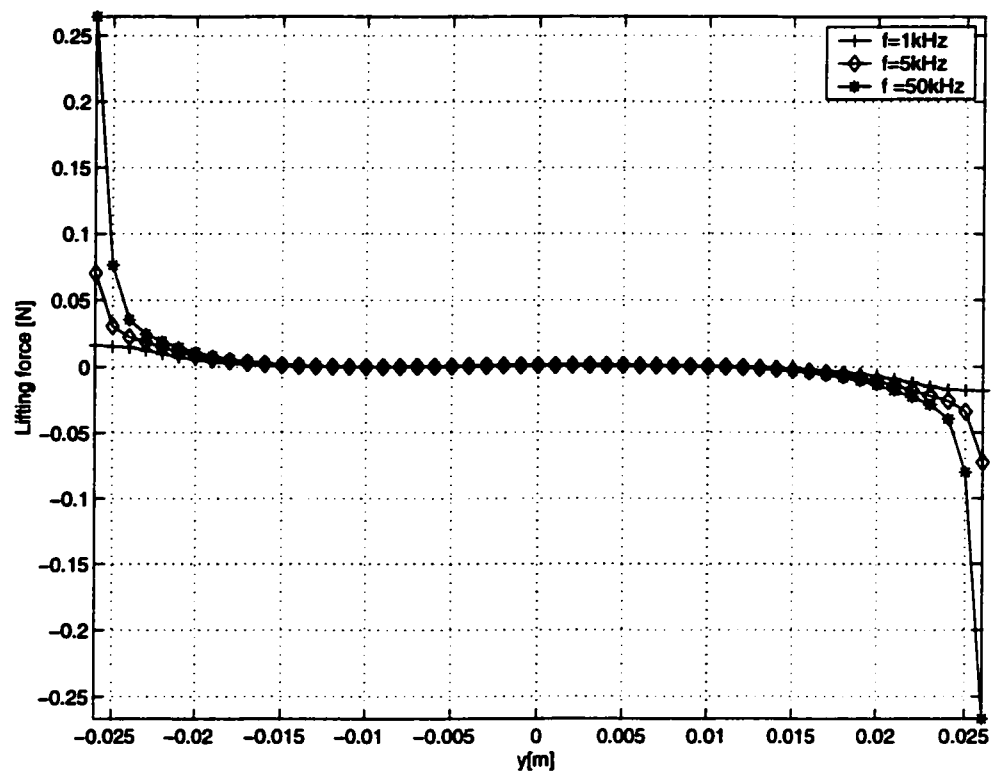
Figure 3.4: The influence of the current frequency on the lifting force at 1,5, and 50 kHz.
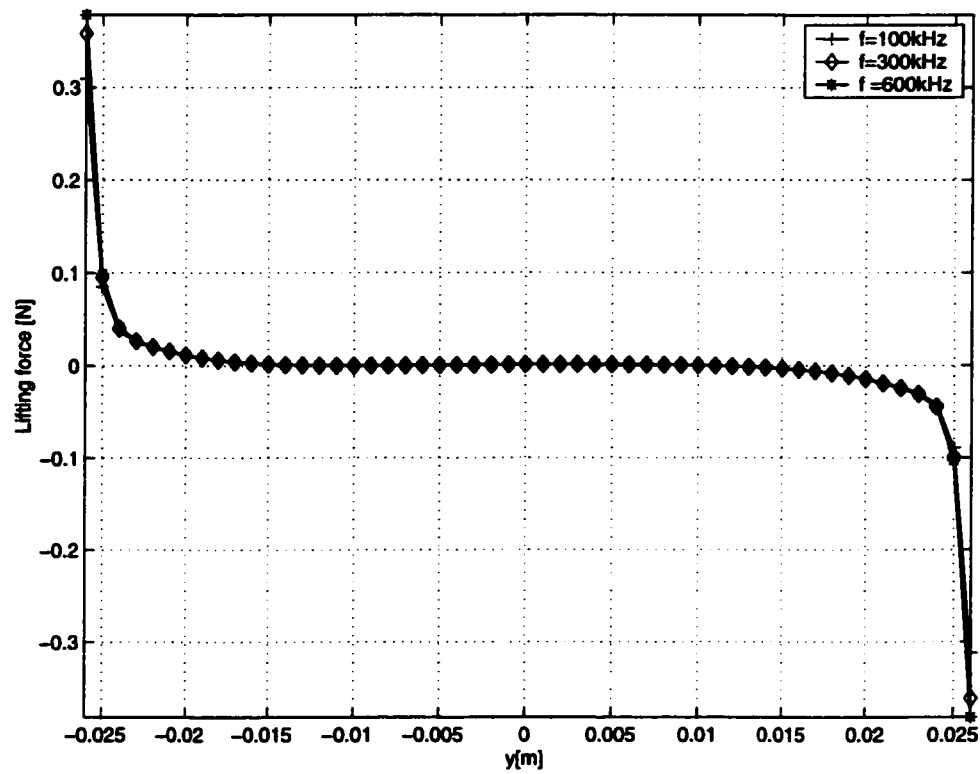
Figure 3.5: The influence of the current frequency on the lifting force at 100, 300, and 600 kHz
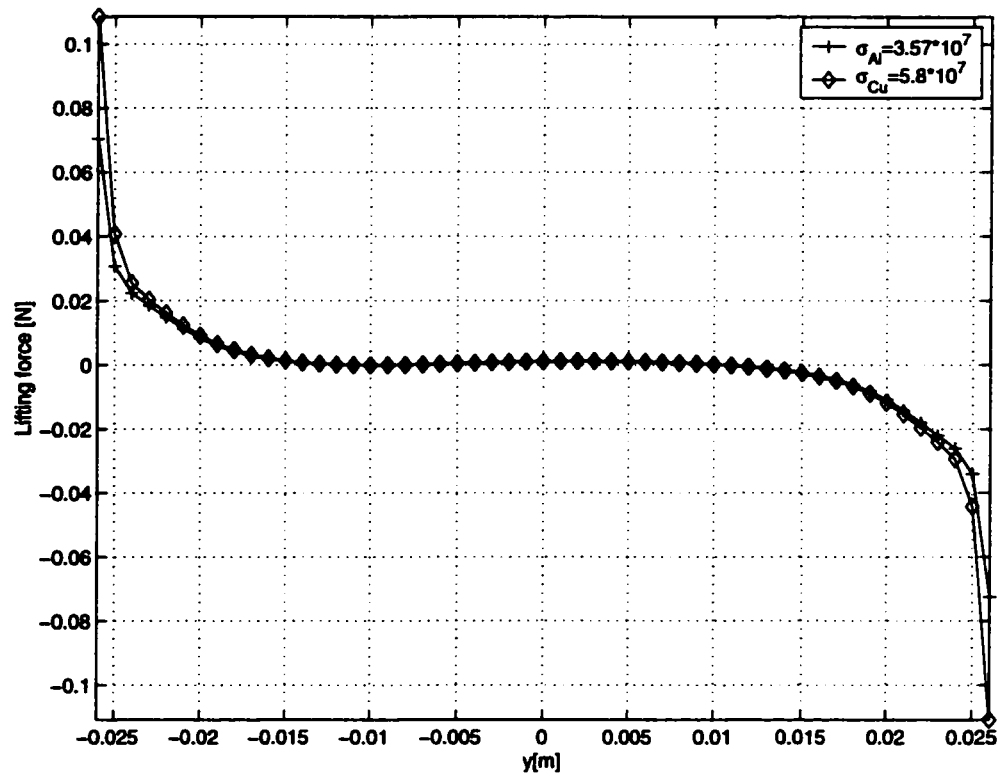
Figure 3.6: The influence of the electrical conductivity on the lifting force at 5kHz.
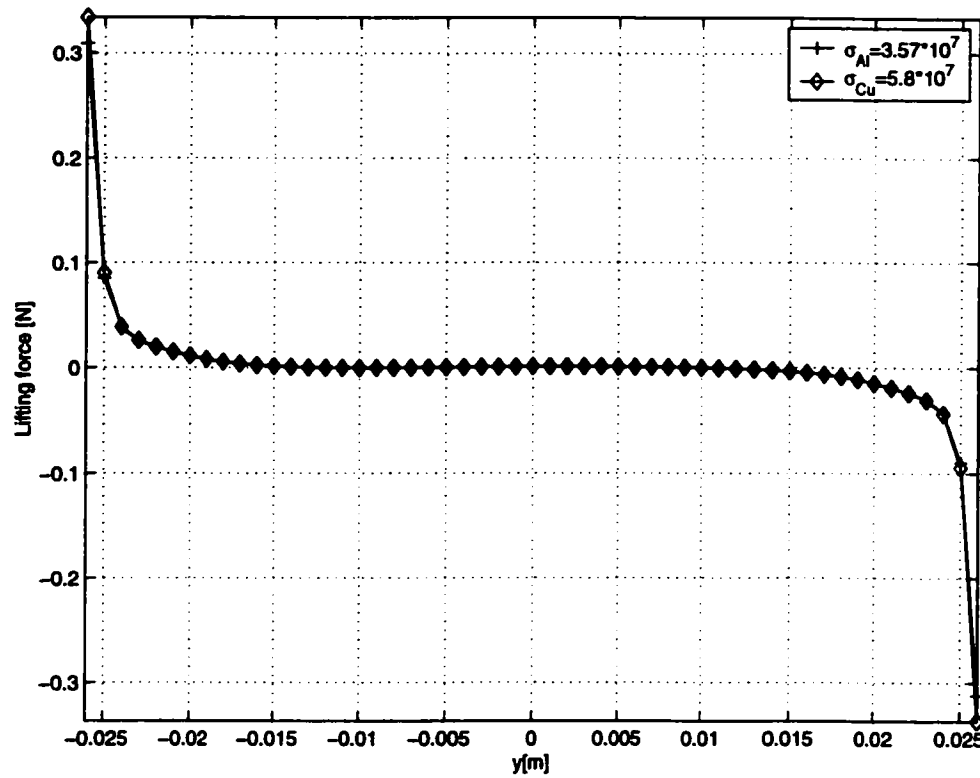
Figure 3.7: The influence of the electrical conductivity on the lifting force at 300kHz.
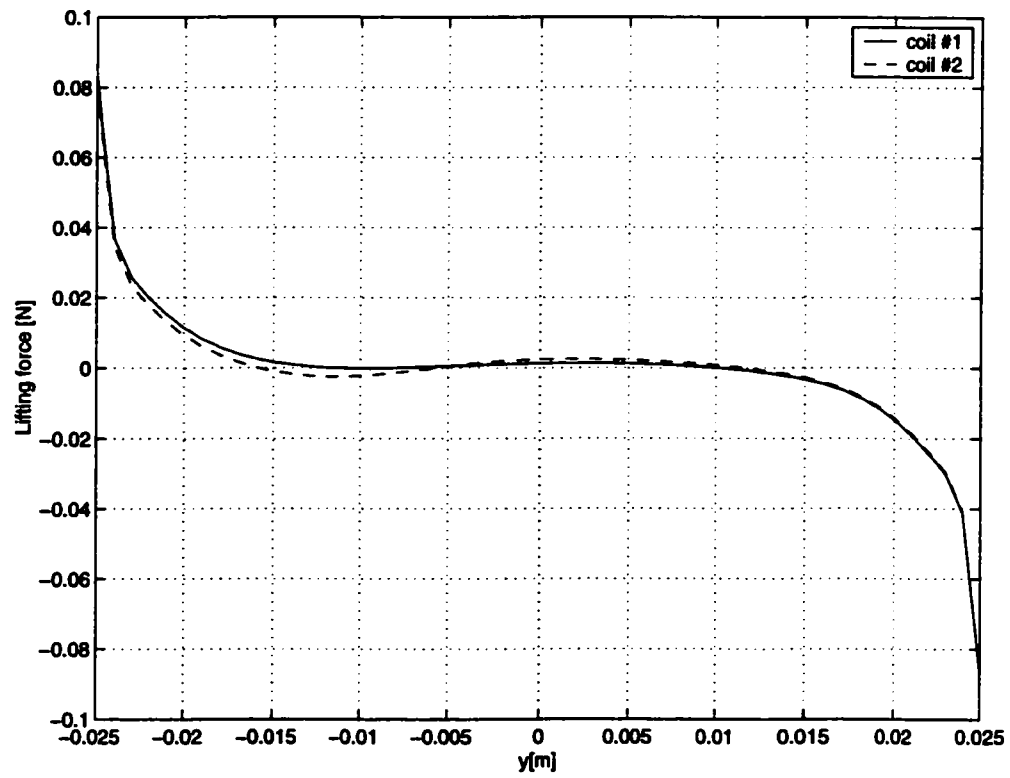
Figure 3.8: The influence of the coil configuration.

3.3 Damping Force Analysis

3.3.1 Damping Force

Shampine [32, 33] reported that horizontal stability was excellent inside of the longitudinal levitator. Because of the longitudinal levitator's vertical symmetry about its centerline, the substantial oscillations of the sample can only be observed in the vertical direction as long as the sample is located along the centerline of the levitator. Therefore, we focus the vertical motion of the sample in this analysis.

The time averaged damping force per unit length, $\mathbf{F}_d^A$, can be defined as

$$\mathbf{F}_d = \frac{1}{2}Re \int_0^{2\pi} \int_0^a \sigma(\mathbf{v} \times \mathbf{B}) \times \mathbf{B}^* r dr d\theta \qquad (3.23)$$

Defining $\mathbf{v} = v_y\mathbf{j}$ as the velocity vector of the sample and $\mathbf{B} = B_x\mathbf{i} + B_y\mathbf{j}$ as the magnetic flux density in Cartesian coordinates, $\mathbf{v} \times \mathbf{B}$ term in Equation (3.23) can be written as

$$\mathbf{v} \times \mathbf{B} = v_y\mathbf{j} \times (B_x\mathbf{i} + B_y\mathbf{j}) \qquad (3.24)$$

where the Cartesian components of $\mathbf{B}$ are

$$\begin{aligned} B_x &= B_r cos\theta - B_\theta sin\theta \\ B_y &= B_r sin\theta + B_\theta cos\theta \end{aligned} \qquad (3.25)$$

substituting Equation (3.25) into Equation(3.24)

$$\mathbf{v} \times \mathbf{B} = v_y(B_\theta sin\theta - B_r cos\theta)\mathbf{k} \qquad (3.26)$$

Using the above result and expanding $\mathbf{B}^*$ in the Cartesian coordinates, Equation (3.23) can be rewritten as

$$\mathbf{F}_d = \frac{\sigma v_y}{2}Re \int_0^{2\pi} \int_0^a (B_\theta sin\theta - B_r cos\theta)\mathbf{k} \times (B_x^*\mathbf{i} + B_y^*\mathbf{j}) r dr d\theta \qquad (3.27)$$

where B_x^* and B_y^* are the complex conjugates of B_x and B_y which are given in Equation (3.25). Therefore, the vertical component of the damping force becomes

$$F_{dy} = \frac{\sigma v_y}{2} Re \int_0^{2\pi} \int_0^a (B_\theta sin\theta - B_r cos\theta)(B_r^* cos\theta - B_\theta^* sin\theta)r dr d\theta \qquad (3.28)$$

and after some algebra

$$F_{dy} = \frac{\sigma v_y}{2} Re \int_0^{2\pi} \int_0^a (B_r B_\theta^* cos\theta sin\theta + B_\theta B_r^* cos\theta sin\theta)r dr d\theta \qquad (3.29)$$

Defining I_1 and I_2 as the first and second terms of the integral in Equation (3.29)

$$I_1 = Re \int_0^{2\pi} \int_0^a B_r B_\theta^* cos\theta sin\theta r dr d\theta \qquad (3.30)$$

and

$$I_2 = Re \int_0^{2\pi} \int_0^a B_\theta B_r^* cos\theta sin\theta r dr d\theta \qquad (3.31)$$

Equation (3.29) can be rewritten as

$$F_{dy} = \frac{\sigma v_y}{2}(I_1 + I_2) \qquad (3.32)$$

Solution of I_1

Substituting the electromagnetic field equations (2.23)(2.24) into Equation (3.30)

$$I_1 = Re \int_0^{2\pi} \int_0^a \sum_{n=-\infty}^{\infty} \sum_{m=-\infty}^{\infty} (\frac{in}{r})C_n J_n(k_1 r)e^{in\theta}(-k_1^*)C_m^* J_m(k_1 r)^* e^{-im\theta} cos\theta sin\theta r dr d\theta \qquad (3.33)$$

Rearranging the terms leads,

$$I_1 = Re[k_1 \sum_{n=-\infty}^{\infty} \sum_{m=-\infty}^{\infty} C_n C_m^* P_{n,m}^{(1)} T_{n,m}] \qquad (3.34)$$

where $P_{n,m}^{(1)}$ is

$$P_{n,m}^{(1)} = n \int_0^a J_n(k_1 r) J_m'(k_1 r)^* dr \qquad (3.35)$$

and $T_{n,m}$

$$T_{n,m} = \int_0^{2\pi} e^{i(n-m)\theta} cos\theta sin\theta d\theta \qquad (3.36)$$

Using Euler's formula, Equation (3.36) can be rewritten as

$$T_{n,m} = \int_0^{2\pi} (cos(n-m)\theta cos\theta sin\theta + isin(n-m)\theta cos\theta sin\theta)d\theta \qquad (3.37)$$

and rearranging the terms leads,

$$T_{n,m} = \frac{1}{2}(\int_0^{2\pi} cos(n-m)\theta sin2\theta d\theta + i \int_0^{2\pi} sin(n-m)\theta sin2\theta d\theta) \qquad (3.38)$$

The result of the first integral is zero, thus

$$T_{n,m} = \frac{1}{2}i \int_0^{2\pi} sin(n-m)\theta sin2\theta d\theta \qquad (3.39)$$

The solution of the above integral is

$$T_{n,m} = \begin{cases} \frac{\pi}{2}i & \text{if } n-m = +2 \\ -\frac{\pi}{2}i & \text{if } n-m = -2 \\ 0 & \text{if } | n-m | \neq 2 \end{cases}$$

Finally, $T_{n,m}$ can be written as

$$T_{n,m} = \frac{i\pi}{2}(\delta_{n,n-2} - \delta_{n,n+2}) \qquad (3.40)$$

where δ is the unit impulse function.

From the recursion formula of Bessel function

$$J_m'(k_1 r)^* = J_{m-1}(k_1 r)^* - \frac{m}{(k_1 r)^*} J_m(k_1 r)^* \qquad (3.41)$$

and substituting Equation (3.41) into Equation(3.35) we can obtain

$$P_{n,m}^{(1)} = n \int_0^a J_n(k_1 r) J_{m-1}(k_1 r)^* dr - \frac{m}{k_1^*} \int_0^a J_n(k_1 r) J_m(k_1 r)^* \frac{dr}{r} \tag{3.42}$$

Finally, substituting Equation (3.40) into Equation(3.33), I_1 can be written as

$$I_1 = Re[k_1^* \frac{\pi}{2} \sum_{n=-\infty}^{\infty} C_n (C_{n-2}^* P_{n,n-2}^1 - C_{n+2}^* P_{n,n+2}^1)] \tag{3.43}$$

Solution of I_2

Substituting the electromagnetic field equations (2.23)(2.24) into Equation (3.31)

$$I_2 = Re \int_0^{2\pi} \int_0^a -k_1 \sum_{n=-\infty}^{\infty} \sum_{m=-\infty}^{\infty} C_n J_n'(k_1 r) e^{in\theta} (\frac{-im}{r}) C_m^* J_m(k_1 r)^* e^{-im\theta} cos\theta sin\theta r dr d\theta \tag{3.44}$$

Rearranging the terms leads,

$$I_2 = Re[-k_1 \sum_{n=-\infty}^{\infty} \sum_{m=-\infty}^{\infty} C_n C_m^* (-i) P_{n,m}^{(2)} T_{n,m}] \tag{3.45}$$

where $P_{n,m}^{(2)}$ is

$$P_{n,m}^{(2)} = m \int_0^a J_n'(k_1 r) J_m(k_1 r)^* dr \tag{3.46}$$

From the recursion formula of Bessel function

$$J_n'(k_1 r) = J_{n-1}(k_1 r) - \frac{m}{(k_1 r)} J_m(k_1 r) \tag{3.47}$$

and substituting Equation (3.44) into Equation(3.43) we can write

$$P_{n,m}^{(2)} = m \int_0^a J_{n-1}(k_1 r) J_m(k_1 r)^* dr - \frac{n}{k_1} \int_0^a J_n(k_1 r) J_m(k_1 r)^* \frac{dr}{r} \tag{3.48}$$

Thus, Equation(3.41) can be written as

$$I_2 = Re[-k_1 \frac{\pi}{2} \sum_{n=-\infty}^{\infty} C_n (C_{n-2}^* P_{n,n-2}^2 - C_{n+2}^* P_{n,n+2}^2)] \tag{3.49}$$

Finally, substituting I_1 and I_2 into Equation (3.46) and Equation (3.40) into Equation (3.32), the vertical component of the damping force can be obtained as

$$
\begin{aligned}
F_{dy} \; = \; & \frac{\sigma v_y}{2} Re[k_1^* \frac{\pi}{2} \sum_{n=-\infty}^{\infty} C_n (C_{n-2}^* P_{n,n-2}^1 - C_{n+2}^* P_{n,n+2}^1) \\
& - k_1 \frac{\pi}{2} \sum_{n=-\infty}^{\infty} C_n (C_{n-2}^* P_{n,n-2}^2 - C_{n+2}^* P_{n,n+2}^2)]
\end{aligned}
\tag{3.50}
$$

3.3.2 Damping Force Simulation Results

Using Equation (3.50), we obtained the relationship of the damping force and the position and the velocity of the sample. In order to analyze the influences of the system parameters on the damping force, we defined a velocity independent damping function, D, as

$$
\begin{aligned}
D = \frac{F_{dy}}{v_y} \; = \; & \frac{\sigma}{2} Re[k_1^* \frac{\pi}{2} \sum_{n=-\infty}^{\infty} C_n (C_{n-2}^* P_{n,n-2}^1 - C_{n+2}^* P_{n,n+2}^1) \\
& - k_1 \frac{\pi}{2} \sum_{n=-\infty}^{\infty} C_n (C_{n-2}^* P_{n,n-2}^2 - C_{n+2}^* P_{n,n+2}^2)]
\end{aligned}
\tag{3.51}
$$

and analysed the effects of the coil geometry, the coil current, current frequency, and the sample's diameter and electrical conductivity on the damping function. In this analysis, the system parameters are the same as those that have been used in Chapter 3.2.2.

Figure 3.9 shows the damping function versus vertical position along the center-line of the 6-poles asymmetric levitator (shown in Fig 2.3b.). The diameter of the aluminum sample is 1.6 cm. As it is seen from the figure, the damping function is negative along the vertical axis, and the absolute value of D is greater at the positions where the sample is close to the coils.

The damping force depends on the square of the coil current. Figure 3.10 illustrates the effect of the coil current on the damping function. As it is seen from the figure, the damping effect is almost lost for small values of the coil current.
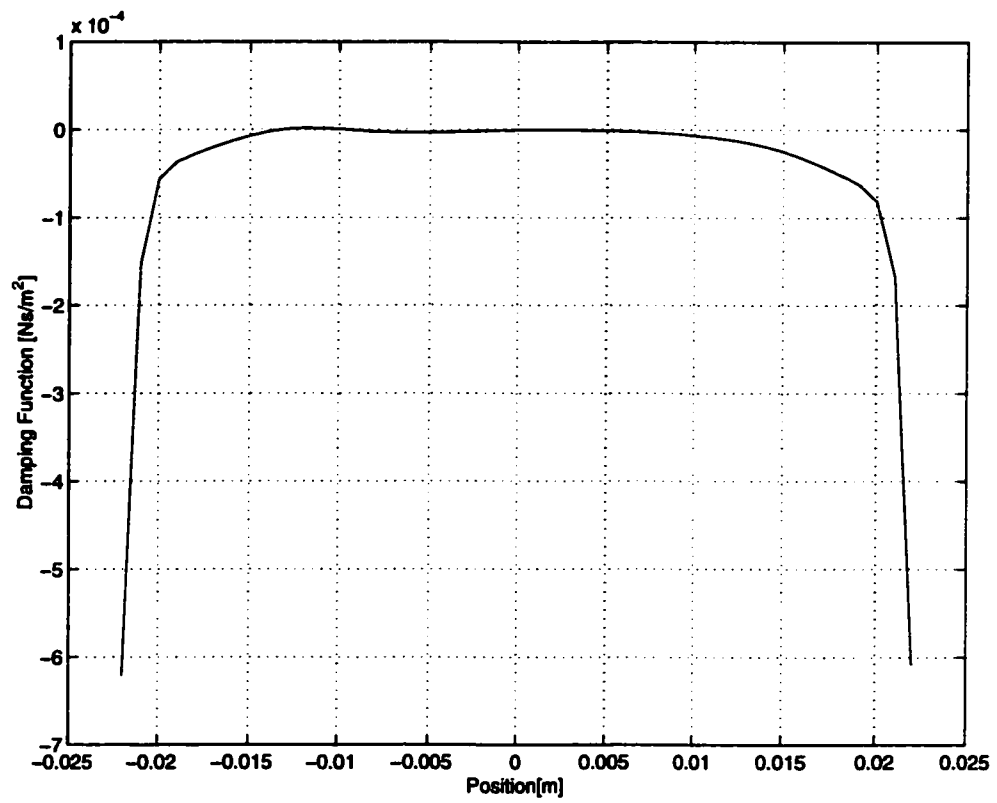
The influence of the sample diameter on the damping function is illustrated in Fig 3.11. It can be seen that the damping force increases as the sample diameter increases.

The influence of the coil frequency on the damping force is different than its influence on the lifting force. As shown in Figure 3.12, the damping effect decreases as the frequency increases. The same behaviour is observed at high frequencies as shown in Figure 3.13 If the sign of the damping function is negative along the vertical axis, the direction of the damping force will be always opposite to the direction of the velocity of the sample during the levitation. This is why F_d is named as damping component of the levitation force.

From Equation (3.50), it can be seen that the magnitude of the damping force depends on the magnitude of the velocity, the position of the sample, the coil current, the coil geometry and the electric conductivity of the sample.

Figure 3.14 shows the influence of the velocity and the position of the sample on the damping force when the other parameters are fixed. As shown, the damping force is stronger in the region where the sample is close to the poles at the bottom and the top of the levitator. On the other hand, the direction of the damping force changes as the direction of the velocity vector changes.

The change in the coil configuration can dramatically change the damping force. Figure 3.15 illustrates the damping force when the two poles in the middle of the levitator are approached 1.2 cm to each other.

Figure 3.9: Damping function versus vertical position.
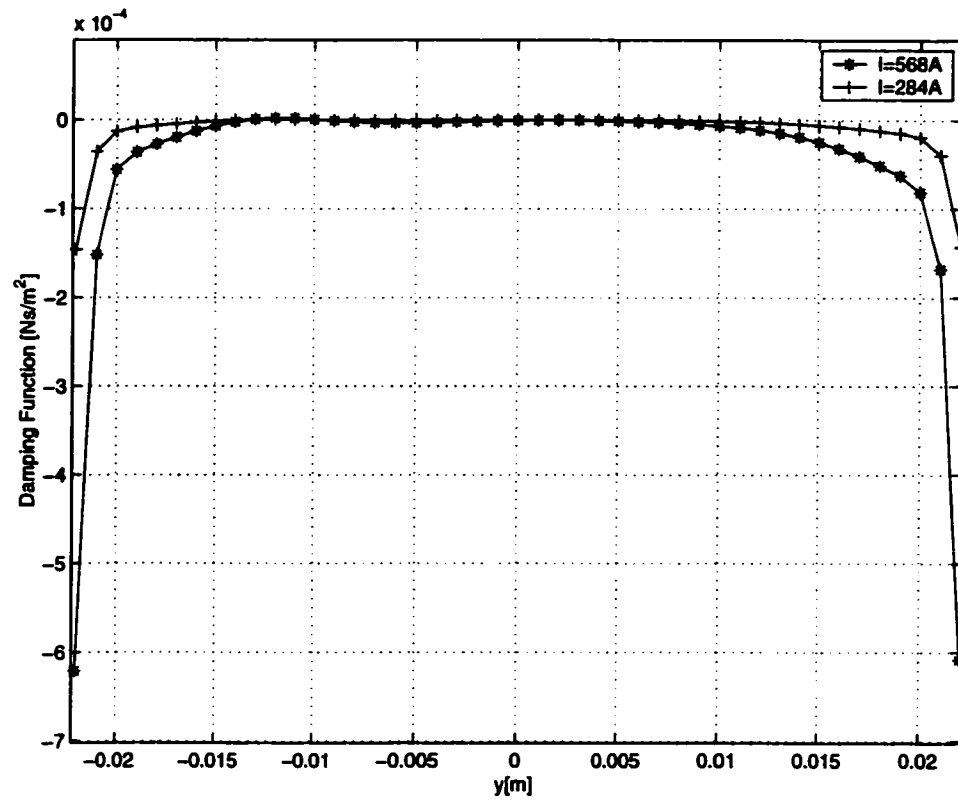
Figure 3.10: The influence of the coil current on the damping function.
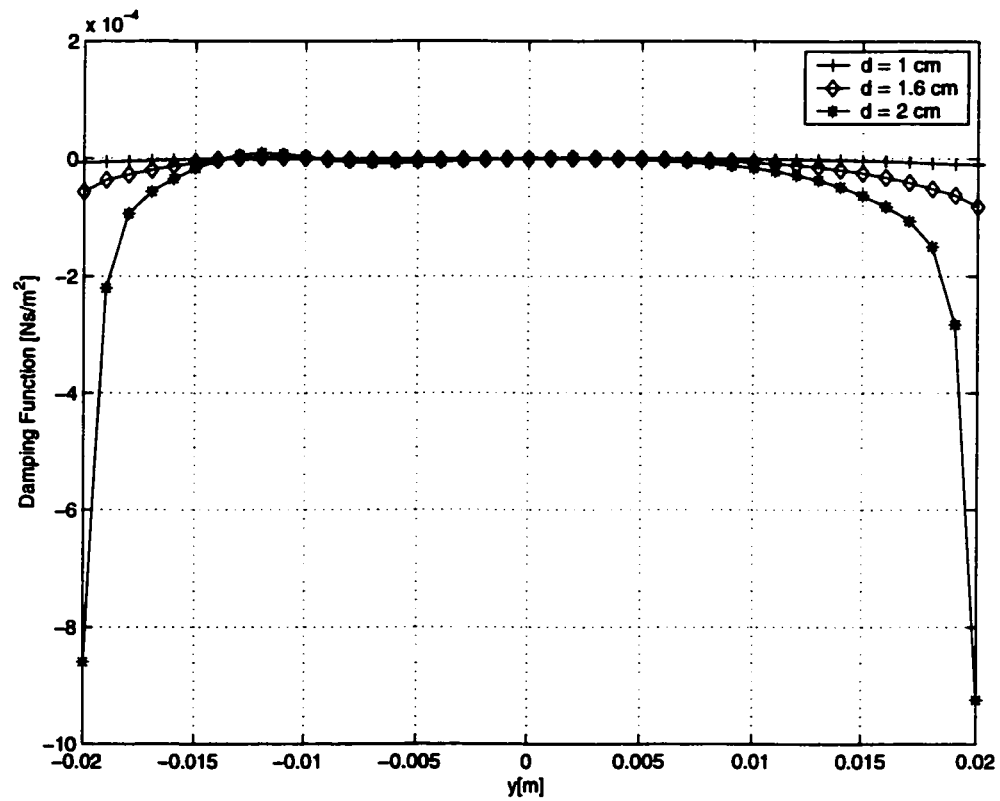
Figure 3.11: The influence of the sample diameter on the damping function.
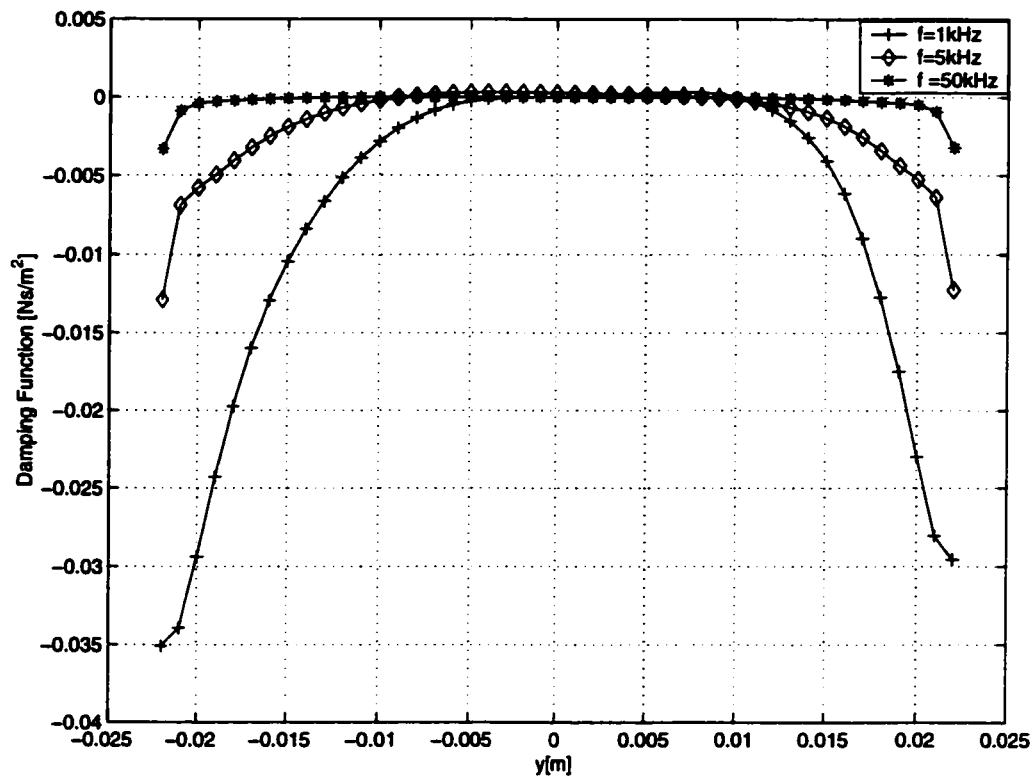
Figure 3.12: The influence of the current frequency on the damping function at 1 kHz, 5 kHz, and 50 kHz.
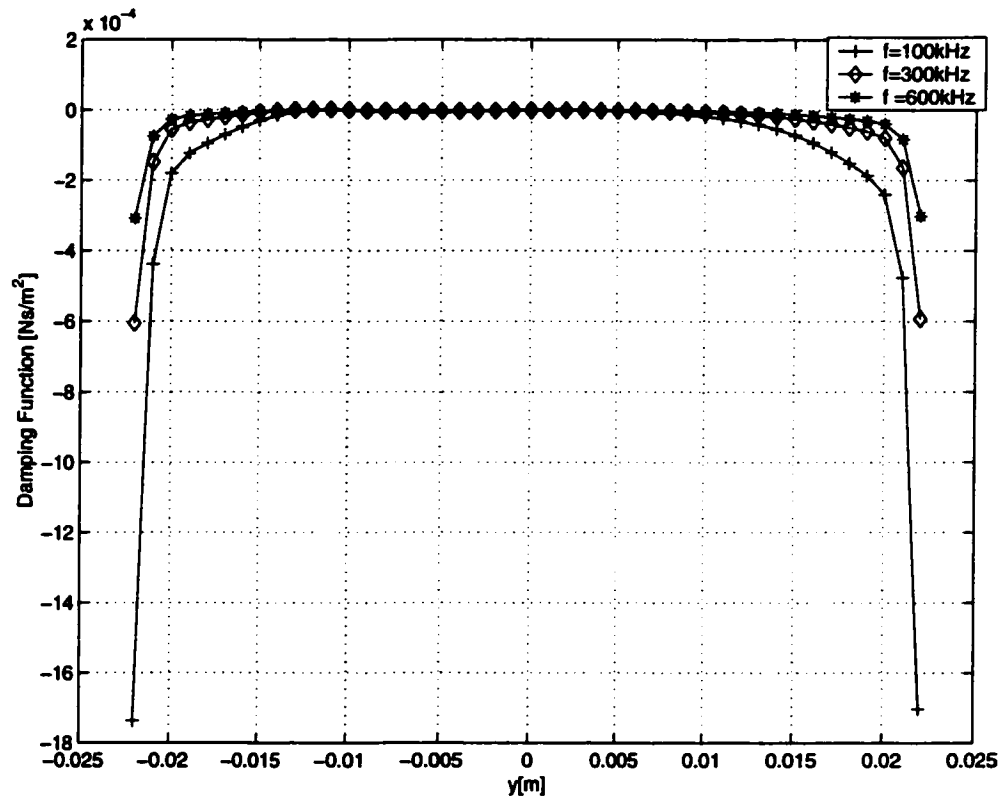
Figure 3.13: The influence of the current frequency on the damping function at 100 kHz, 300 kHz, and 600 kHz.
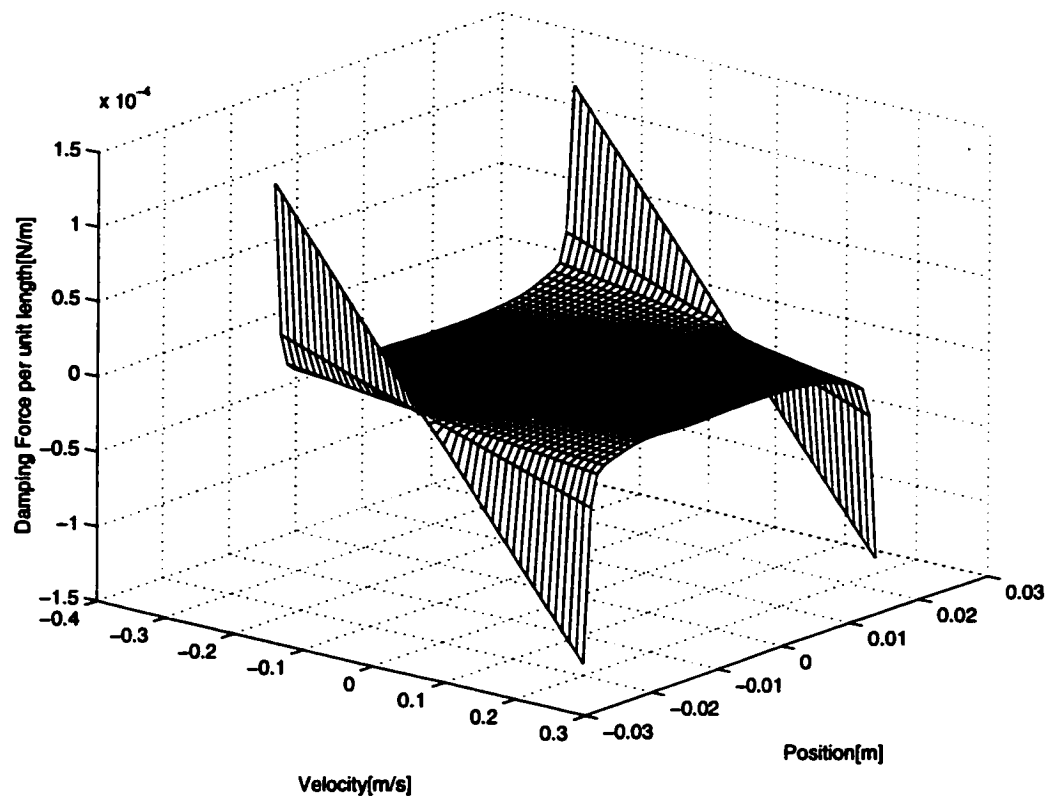
Figure 3.14: The influence of the position and the velocity of the sample on the damping force.
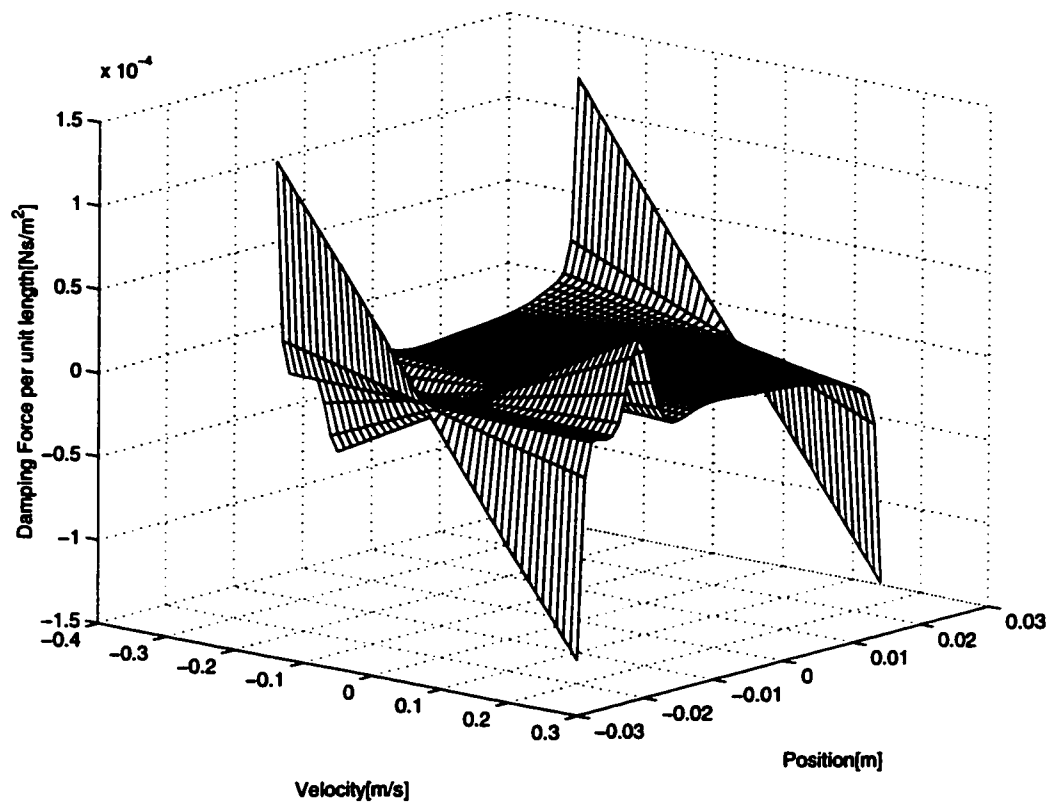
Figure 3.15: The influence of the coil configuration on the damping force.

Chapter 4

Dynamical Analysis and Control

In this chapter, using the results of the lifting and damping force analysis, we obtained a dynamical model of the levitated sample's motion. In order to analyze the sample's open loop dynamical behaviour, and the effects of the system parameters on the sample's motion, the model was transformed into the state-space form. Using the Runge-Kutta algorithm, the position and the velocity trajectories were obtained. To achieve stable levitation, two feedback control techniques, the PD based and the pole-placement, were implemented and several simulations were performed to evaluate the controllers' performances.

4.1 State-space form

Considering both the lifting and the damping components of the levitation force, which were derived in the previous chapter, and assuming that the levitated sample stays in solid state, a force balance analysis in the vertical plane yields the following equation of the motion for a given sample

$$m\ddot{y} = F_{ly}(y, \hat{I}_m) + D(y, \hat{I}_m)\dot{y} - mg \tag{4.1}$$

where m is the mass of the sample, y is distance from the center of the levitator axes in the vertical plane, and g is the gravitational constant. One should notice that both F_{ly} and D are the function of the square of the coil current, and the position of the sample. Substituting F_{ly} and D from equation (3.22) and equation (3.51) into equation (4.1), the equation of the motion becomes

$$m\ddot{y} = Im\{\frac{\mu_0 \hat{I}_m^2}{4\pi a}\sum_{n=1}^{\infty}[\{\sum_{m=1}^{p}(\frac{a}{c_m - iy})^n\}\{\sum_{m=1}^{p}(\frac{a}{c_m^* + iy})^{n+1}\}Re\frac{J_{n+1}(k_1 a)}{J_{n-1}(k_1 a)}]\} +$$

$$\frac{\sigma}{2}Re[k_1^*\frac{\pi}{2}\sum_{n=-\infty}^{\infty}C_n(C_{n-2}^* P_{n,n-2}^1 - C_{n+2}^* P_{n,n+2}^1) - k_1\frac{\pi}{2}\sum_{n=-\infty}^{\infty}C_n(C_{n-2}^* P_{n,n-2}^2$$

$$- C_{n+2}^* P_{n,n+2}^2)]\dot{y} - mg \qquad (4.2)$$

To analyze the dynamics of the system, a numerical integration method should be used. When the state variables $x_1 = y$, $x_2 = dy/dt$ are introduced, the state-space model of the system becomes

$$\dot{x}_1 = x_2$$

$$\dot{x}_2 = (Im\{\frac{\mu_0 \hat{I}_m^2}{4\pi a}\sum_{n=1}^{\infty}[\{\sum_{m=1}^{p}(\frac{a}{c_m - ix})^n\}\{\sum_{m=1}^{p}(\frac{a}{c_m^* + ix})^{n+1}\}Re\frac{J_{n+1}(k_1 a)}{J_{n-1}(k_1 a)}]\} +$$

$$\frac{\sigma}{2}Re[k_1^*\frac{\pi}{2}\sum_{n=-\infty}^{\infty}C_n(C_{n-2}^* P_{n,n-2}^1 - C_{n+2}^* P_{n,n+2}^1) - k_1\frac{\pi}{2}\sum_{n=-\infty}^{\infty}C_n(C_{n-2}^* P_{n,n-2}^2$$

$$- C_{n+2}^* P_{n,n+2}^2)]x_2 - mg)/m \qquad (4.3)$$

The Runge-Kutta algorithm in MATLAB has been used to perform the integration.

4.2 Dynamical Model Simulation Results

Several simulations were performed in order to determine qualitatively the behavior of the sample levitated by the longitudinal levitator. The system parameters are same as those that have been used in the previous chapter.

Because the force balance is provided only at the equilibrium points, the sample will oscillate unless it is not accurately released at its equilibrium position before the levitation starts. Figure 4.1 illustrates the effect of the initial position on the sample's dynamic behaviour. In the figure, Δx represents the difference betweeen the initial and the equilibrium positions, which is -20.7 mm for the selected sample. The two diagrams in the figure show the trajectory of the position and the velocity of

the sample, respectively. Even a very small deviation from the equlibrium can cause substantial oscillations of the sample as shown in the figure. This result was also experimentally found in [38, 39].

According to Equation (3.50), the magnitude of the damping force is relatively small when compared with the lifting force. Figure 4.2 illustrates the effect of the damping force on the sample's motion for the time interval of 15 seconds. It can be concluded that there is a very light damping in the system.

Figure 4.3 illustrates the influence of the coil current on both the lifting force and the sample's dynamics. The first and the second diagrams show the trajectory of the position and the velocity of the sample, respectively, and the third diagrams displays the lifting force during the time interval of 0.5 seconds. As it has been discussed in Chapter 3, both the lifting and damping force are proportional to the square of the coil current. On the other hand, only the lifting force has significant effect on the sample's dynamics as it was discussed above. When the coil current is increased by 1.5 times, the lifting force increases 2.25 times according to Equation (3.22). Therefore,the change in the lifting force will dramatically change the oscillation pattern of the sample as can be seen in Figure 4.3.

As it has previously been discussed in the lifting force analysis, the coil configuration can significantly affect the sample's dynamics. Figure 4.4 shows the influence of the coil configuration on the sample's motion. In the figure, coil 1 and coil 2 represent the original and the modified levitators, which have been described in Chapter 3.3.2.

4.3 Feedback Control

The main control task is to achieve stable levitation eliminating the sample's undesired oscillations. Assuming that the system variables such as the position and the

velocity of the sample are available for feedback, and the current can be changed in the system, two control techniques were implemented to achieve a stable levitation.

4.3.1 PD-based control

Most of the feedback algorithm used in current control systems are implementation of a proportional plus derivative (PD) control. The advantages of using a PD controller are the following:

- Very simple to implement.

- No need to have a system model.

- Suitable for real-time control since it has very few computations.

- The behavior of the system can be controlled by changing the feedback gains.

However, it should be noted that PD control cannot guarantee stability when applied to nonlinear systems.

In this analysis, an effort is made to utilize the developed system dynamic equations in deriving a PD-based control law. The dynamic equation of the levitated sample derived in the previous section are written in the form

$$m\ddot{y} = F_{ly}(y, u) + D(y, u)\dot{y} - mg \qquad (4.4)$$

where u is the applied coil current. Using a PD-based control strategy, u can be written in the form as

$$u = K_p(y_d - y) - K_d\dot{y} + u_d \qquad (4.5)$$

where K_p and K_d are the proportional and derivative feedback gains, y_d is the desired levitation position of the sample, and u_d is the value of the coil current, which provides the desired levitation position for the sample. Because the levitation position of the

sample depends only on the coil current when the other system parameters are fixed, the selection of y_d provides the value of u_d by using equation (3.22).

The proportional and the derivative feedback gains were selected as $K_p = K_d = 1000$ by trial and error for $y_d = -20.7mm$. Figure 4.5 shows the state trajectory and the control history. As it is seen from the figure, the sample's oscillations are eliminated within 0.4 seconds.

To evaluate the controller's performance for different levitation positions, several simulations were performed. Figure 4.6 shows the state and the control trajectories for $y_d = -18mm$ and $y_d = -15mm$. As can be seen, the selected feedback gains could not provide the same performance for these positions. This result implies a need to improve the control performance for different levitation positions.

4.3.2 Linear Control Design

In this section, first the equation of the motion is linearized about the designed equilibrium. Then the pole-placement approach is applied to design a linear controller that achieves stable levitation.

Linearization Linearization is a very important approach to the control design of nonlinear systems. Since the equations of the motion are analytic and time-invariant, in some small region in the vicinity of an equilibrium, the behaviour of the system can be approximated with a linear model. In addition, computing the eigenvalues of the linear model it is possible to indicate the stability of the equilibrium points [18, 36].

Assuming that we control the lifting force by varying the current such that the sample is stable corresponding to an equilibrium $x = x_{eq}$ and $\dot{x} = 0$. Defining the deviation from the equilibrium as

$$q = \begin{bmatrix} q_1 \\ q_2 \end{bmatrix} = \begin{bmatrix} x - x_{eq} \\ \dot{x} \end{bmatrix} \tag{4.6}$$

and the dynamics of the deviation of the sample from the equilibrium is given by

$$\dot{q} = \begin{bmatrix} q_2 \\ \dfrac{F_{ly}(q_1, \hat{I}_m) + D(q_1, \hat{I}_m)q_2 - mg}{m} \end{bmatrix} \tag{4.7}$$

where $F_{ly}(q_1, \hat{I}_m)$, and $D(q_1, \hat{I}_m)$ are the expressions of the lifting and the damping force in terms of q. Equation (4.7) can be approximated to first order with linear differential system

$$\dot{q} = A(q_{eq})q \tag{4.8}$$

where $A(q_{eq})$ is the Jacobian matrix

$$A(q_{eq}) = \begin{bmatrix} \dfrac{\partial \dot{q}_1}{\partial q_1} & \dfrac{\partial \dot{q}_1}{\partial q_2} \\ \dfrac{\partial \dot{q}_2}{\partial q_1} & \dfrac{\partial \dot{q}_2}{\partial q_2} \end{bmatrix} = \begin{bmatrix} 0 & 1 \\ A_{21} & A_{22} \end{bmatrix}_{q = 0} \tag{4.9}$$

where

$$A_{21} = Im\{\frac{\mu_0 \hat{I}_m^2}{4\pi a} \sum_{n=1}^{\infty}\{\sum_{m=1}^{p}(\frac{a}{c_m - i(q_1 + x_{eq})})^n \frac{a^{n+1}(n+1)i}{[c_m^* + i(q_1 + x_{eq})]^{n+2}} +$$

$$\frac{na^n(-i)}{[c_m - i(q_1 + x_{eq})]^{n+1}}(\frac{a}{c_m^* + i(q_1 + x_{eq})})^{n+1}\}Re\frac{J_{n+1}(k_1 a)}{J_{n-1}(k_1 a)}\}$$

and

$$A_{22} = \frac{\sigma}{2}Re\{k_1^* \frac{\pi}{2} \sum_{n=-\infty}^{\infty} C_n(C_{n-2}^* P_{n,n-2}^1 - C_{n+2}^* P_{n,n+2}^1) - k_1 \frac{\pi}{2} \sum_{n=-\infty}^{\infty} C_n(C_{n-2}^* P_{n,n-2}^2 -$$

$$C_{n+2}^* P_{n,n+2}^2)\}q_2$$

In the analysis, the equilibrium point was chosen as $x_{eq} = -20.7mm$. Thus, the Jacobian matrix becomes

$$A = \begin{bmatrix} 0 & 1 \\ -3946.7 & -0.0182 \end{bmatrix} \tag{4.10}$$

The eigenvalues of the system are $\lambda = -0.0091 \pm 62.83i$. Therefore, it can be expected that the equilibrium to be a stable focus with a frequency of approximetely 62.83 rad/sec or a period of 0.1 second. The oscillation period agrees well with the results obtained in the previous section. Figure 4.7 illustrates the state-space trajectories for the non-linear model in equation (4.3) with the following initial conditions. I.C. : $x_1 = -22mm, x_2 = 0$ and $\hat{I}_m = 568$ A, 800 A, and 1000 A. (The initial condition of the sample in the levitator is illustrated in Figure 4.8)

Linear control design with Pole Placement The control task is to design a controller lifting force $F(q)$ such that the equilibrium is asymptotically stable.

The equation of the motion in terms of state variable $\mathbf{q}$ was given in equation (4.7). If the sample is at an equilibrium (if $\mathbf{q} = 0$), then the required lifting force F_{eq} to maintain it at the equilibrium is, from equation (4.7),

$$F_{eq} = mg \tag{4.11}$$

Note that when perturbed from the equilibrium,

$$\mathbf{q} = \mathbf{q_{eq}} + \delta\mathbf{q} = \delta\mathbf{q} \tag{4.12}$$

since $\mathbf{q_{eq}} = 0$. Similarly,

$$F = F_{eq} + \delta F \tag{4.13}$$

Noting that $\dot{q}_{eq} = 0$, it follows that

$$\delta\dot{\mathbf{q}} = \mathbf{A}(q_{eq})\delta\mathbf{q} + \mathbf{B}(q_{eq})\delta F + H.O.T. \tag{4.14}$$

where

$$\mathbf{B}(q_{eq}) = \begin{bmatrix} 0 \\ \frac{1}{m} \end{bmatrix} \tag{4.15}$$

and H.O.T. signifies higher order terms. Assuming that H.O.T. are small, the input, δF, could be designed based on the linear model [16],

$$\delta\dot{\mathbf{q}} = \mathbf{A}(\mathbf{q_{eq}})\delta\mathbf{q} + \mathbf{B}(\mathbf{q_{eq}})\delta F \tag{4.16}$$

In pole placement technique, the controller is designed as a linear function of the state variables such that the poles of the corresponding closed loop system have prescribed values. Since the controllability matrix

$$\mathbf{M} = \begin{bmatrix} \mathbf{B} & \mathbf{AB} \end{bmatrix} \tag{4.17}$$

is full rank, it follows that the control law

$$\delta F = -\mathbf{K}\delta\mathbf{q} \tag{4.18}$$

will ensure that the system matrix, $[\mathbf{A} - \mathbf{BK}]$, assumes those prescribed eigenvalues [19]. The choice of the closed loop poles was determined from the desire to have a step response with a settling time < 0.2 sec and the damping ratio of about 0.9. Therefore, the closed loop poles are located at $\mu_{1,2} = -40 \pm 20i$. We used MATLAB function '$place.m$' to compute the feedback gains for an equilibrium of $x_{eq} = -20.7mm$. The gain matrix, $\mathbf{K}$, was computed as

$$\mathbf{K} = \begin{bmatrix} -10.512 & 0.431 \end{bmatrix} \tag{4.19}$$

One should notice that the value of the controller lifting force can be always converted to the corresponding controller current by equation (3.22). Figure 4.9 illustrates the state trajectory and the control history for a simulation with initial condition $x(0) = -22mm$, $\dot{x}(0) = 0$. As can be seen, the sample oscillations could be succesfully eliminated within 0.15 sec.

It should be pointed out that the linearization and the computation of the gain matrix should be repeated for a different levitation position since the pole placement technique promises stability only for the neighborhood of the designed equilibrium. Figure 4.10 illustrates the state and control trajectories for the simulations with desired levitation position $x_{eq} = -18mm$, and $x_{eq} = -15mm$. The gain matrices for

these levitation positions were calculated as

$$\mathbf{K}_{x_{eq}=-18} = \begin{bmatrix} -12.525 & 0.431 \end{bmatrix}$$

$$\mathbf{K}_{x_{eq}=-15} = \begin{bmatrix} -14.392 & 0.432 \end{bmatrix}$$

In addition, as it can be seen in Figure 4.10 the corresponding current values are also reasonable for the levitation process. Based on these results, it can be concluded that the pole-placement technique can be effectively used for the stabilization of the longitudinal levitation process.

4.4 Summary

The understanding of the dynamical behaviour of the levitated sample is of great significance when dealing with stable levitation. In this chapter, combining both the lifting and the damping component of the levitation force, a complete dynamical model of the sample has been developed in vertical direction. The experimental results show the validity of the calculations for the levitation force.

Several simulations were performed to determine the influences of the initial condition, coil current, coil configuration, and the damping force on the sample's motion. The effect of the damping force on the sample's dynamics was found relatively small but not eligible when it is compared with the lifting force.

Based on the dynamical model, two control design technique were proposed to achieve stable levitation. Applying a PD based control law, the sample oscillations could be elimanated within 0.4 sec for $y_d = -20.7mm$. However, the control parameters, which were selected by trial and error, could not provide the same performance for different levitation positions.

To improve the overall performance of the control system, the pole-placement, a linear control design technique, has been succesfully implemented and the effectivness

of this tecnique has been verified with several simulations. Assuming that the system variables are available for feedback, it is concluded that the pole-placement technique can be effectively used to achieve stable levitation.

The results of this analysis may provide a framework for further investigations of the sample's stability and control in the longitudinal levitator.
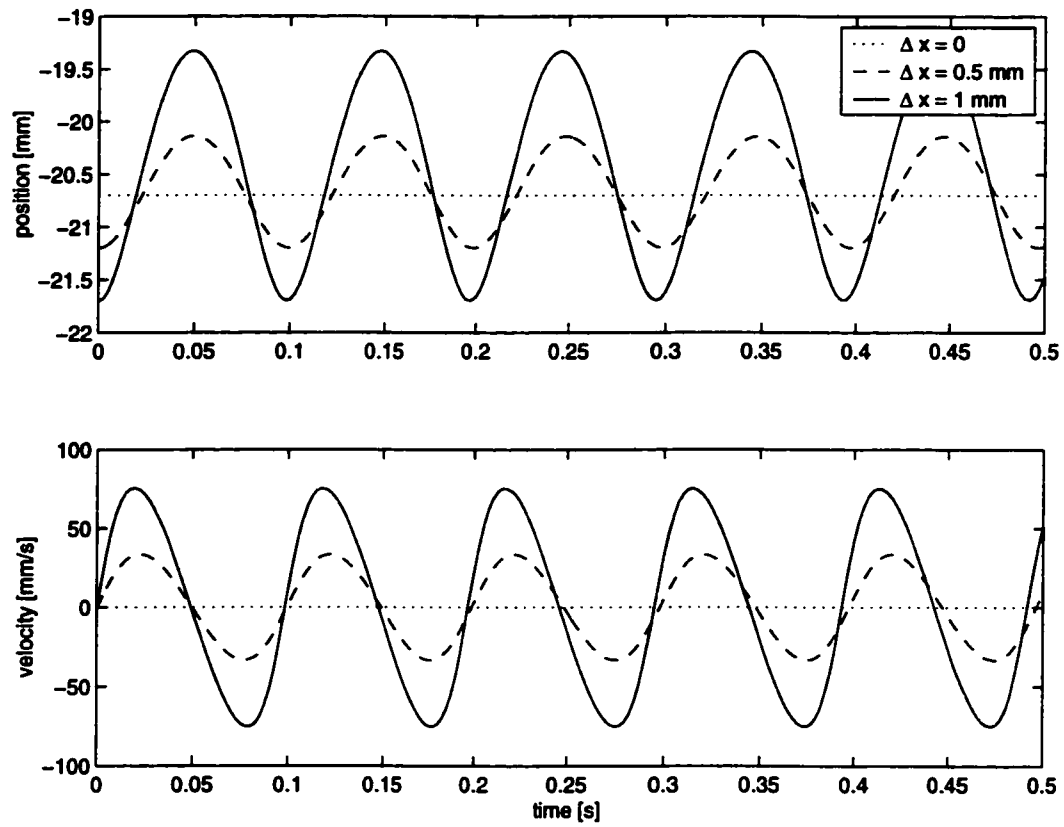
Figure 4.1: The effect of the initial position on the sample's dynamics behaviour.
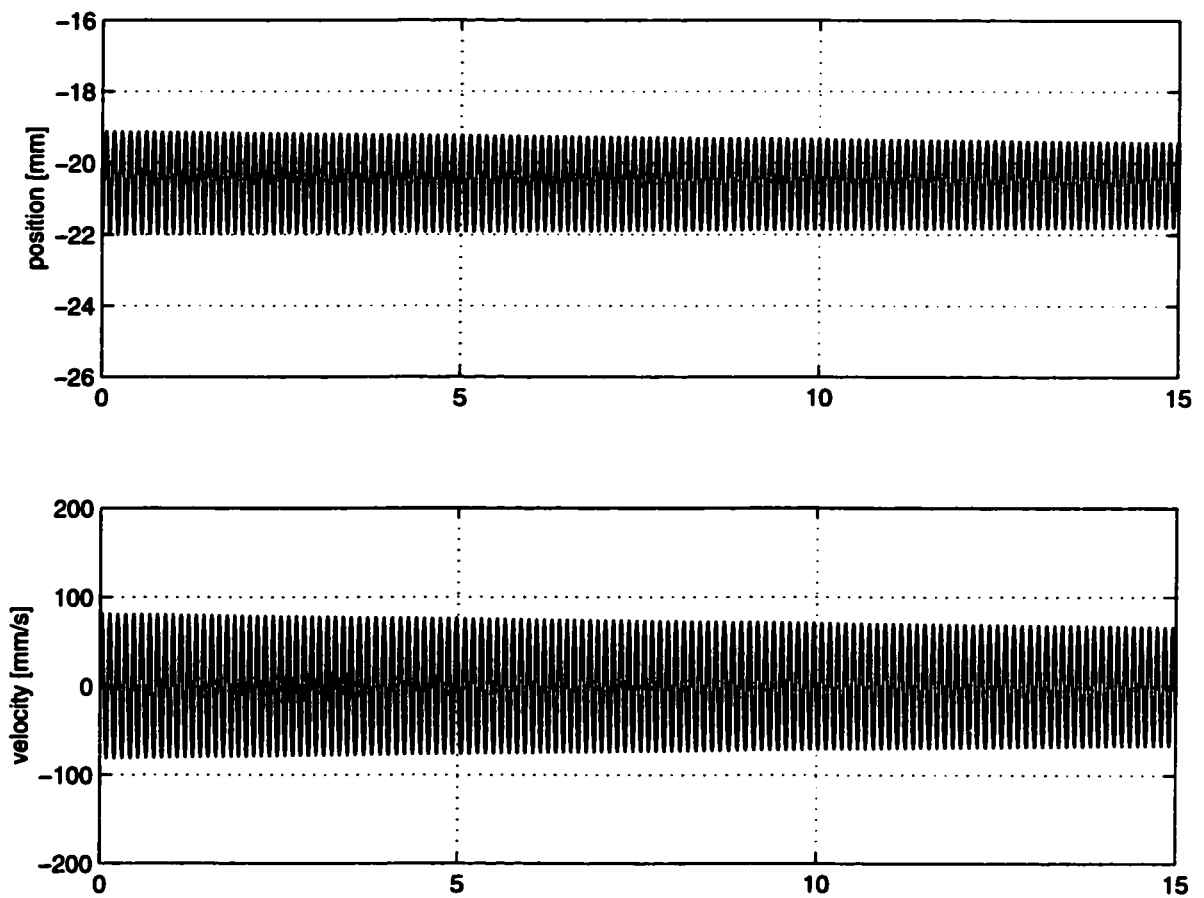
Figure 4.2: The effect of the damping force.
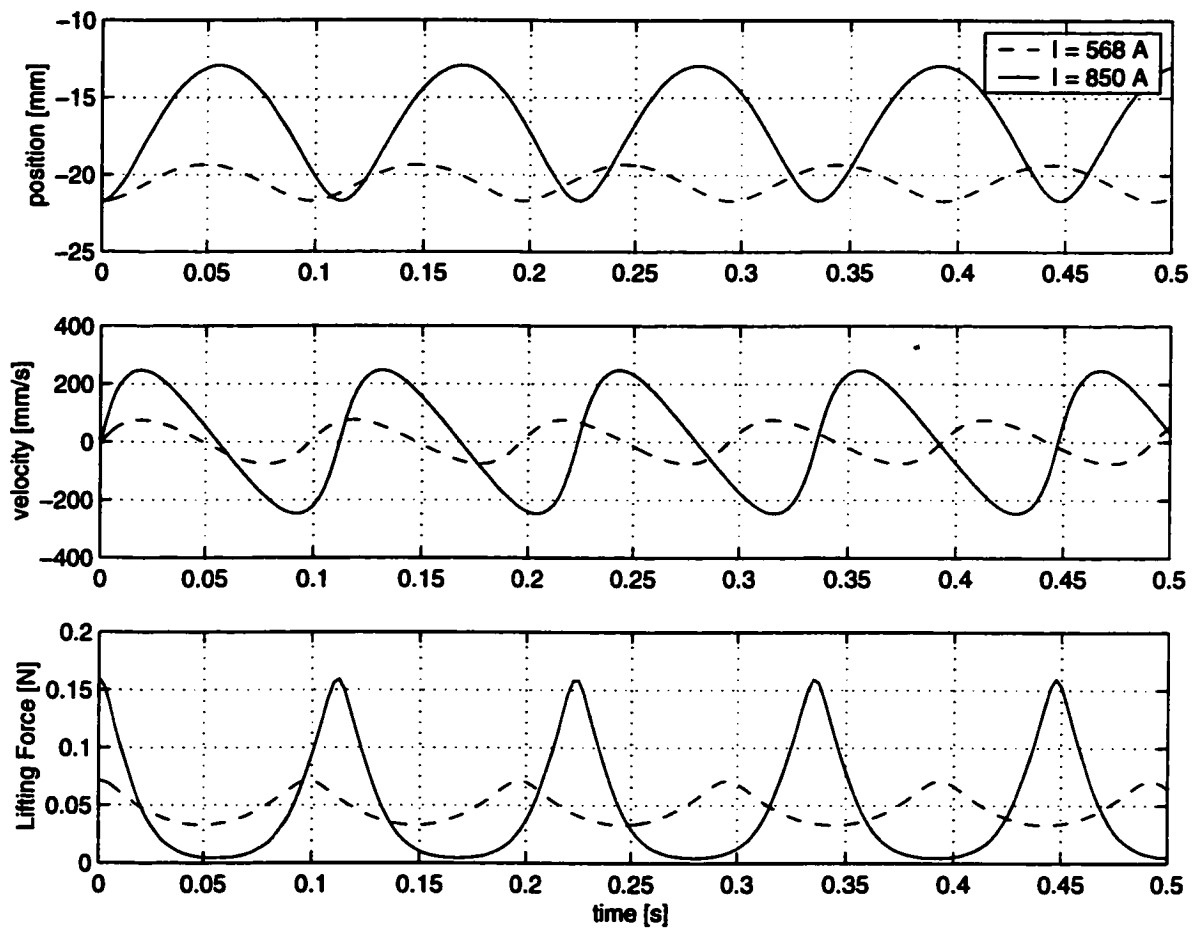
Figure 4.3: The effect of the coil current on the sample's dynamics.
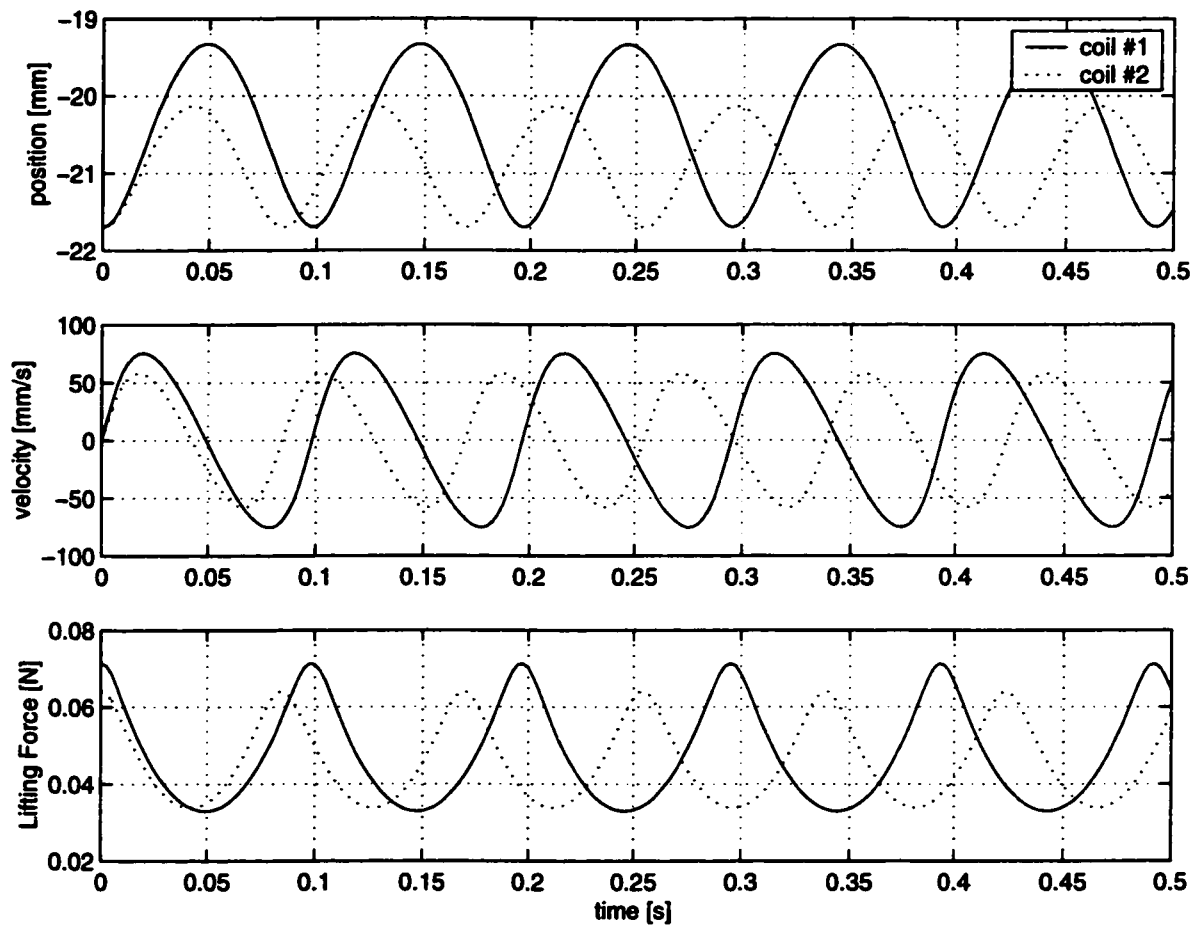
Figure 4.4: The influence of the coil configuration on the sample's motion.
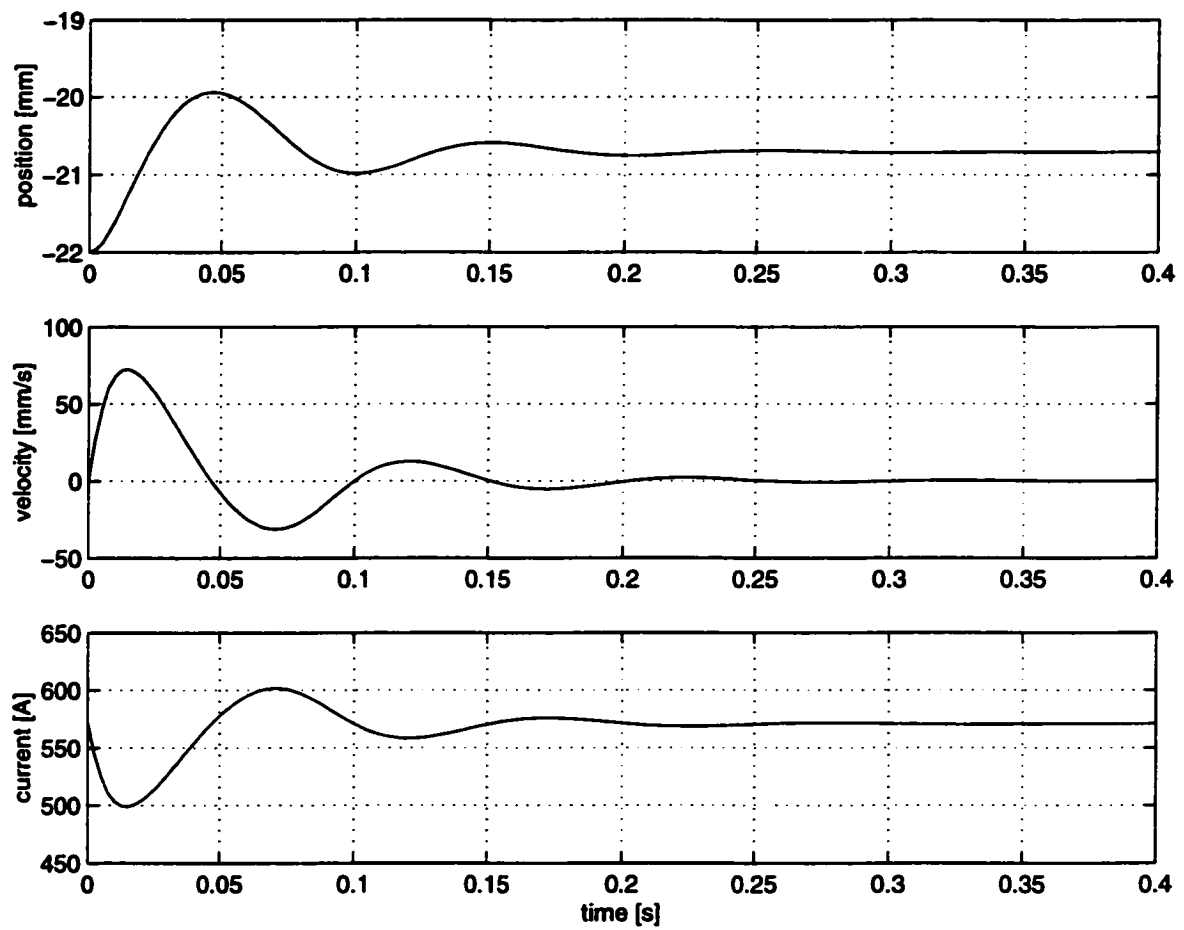
Figure 4.5: PD-based control for y_d= -20.7mm.
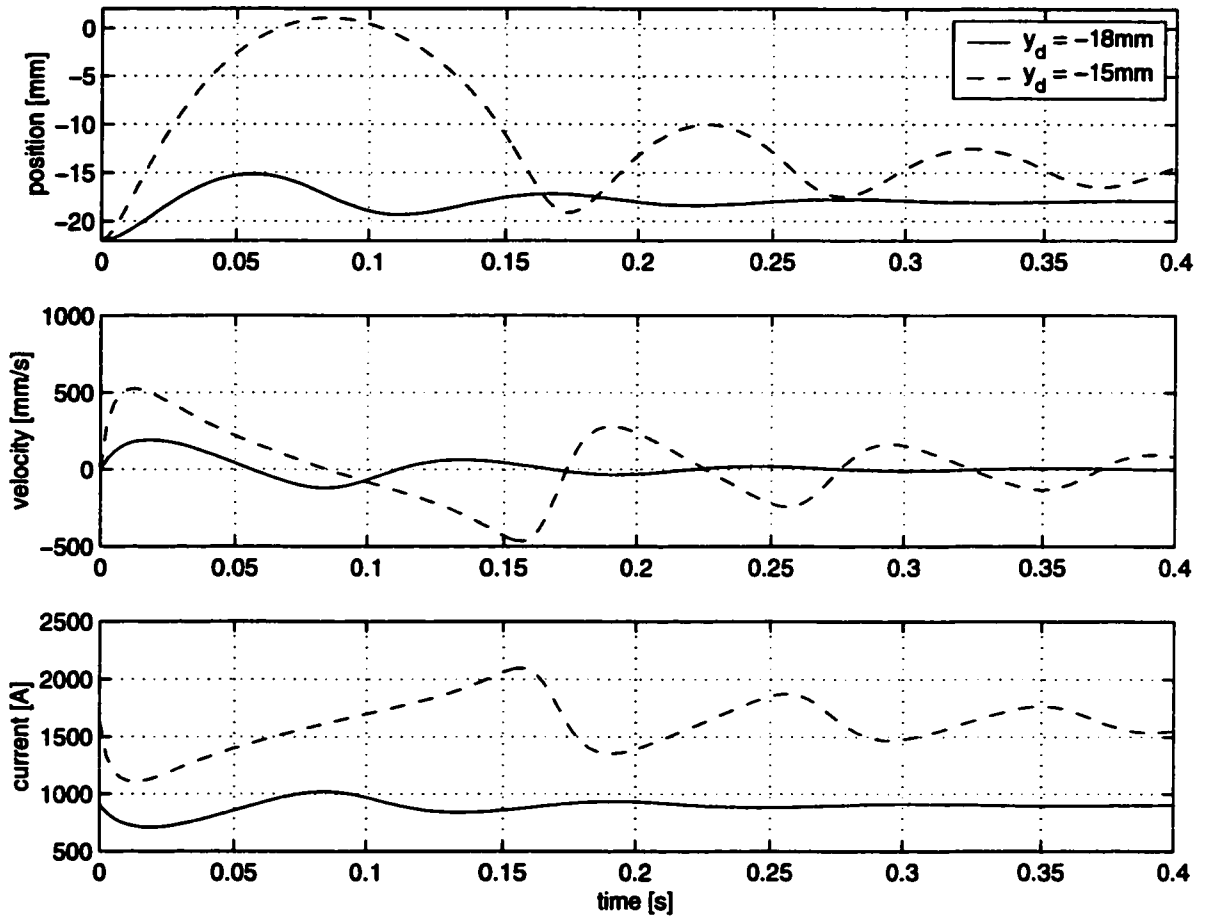
Figure 4.6: PD-based control for the larger values of the levitation position.
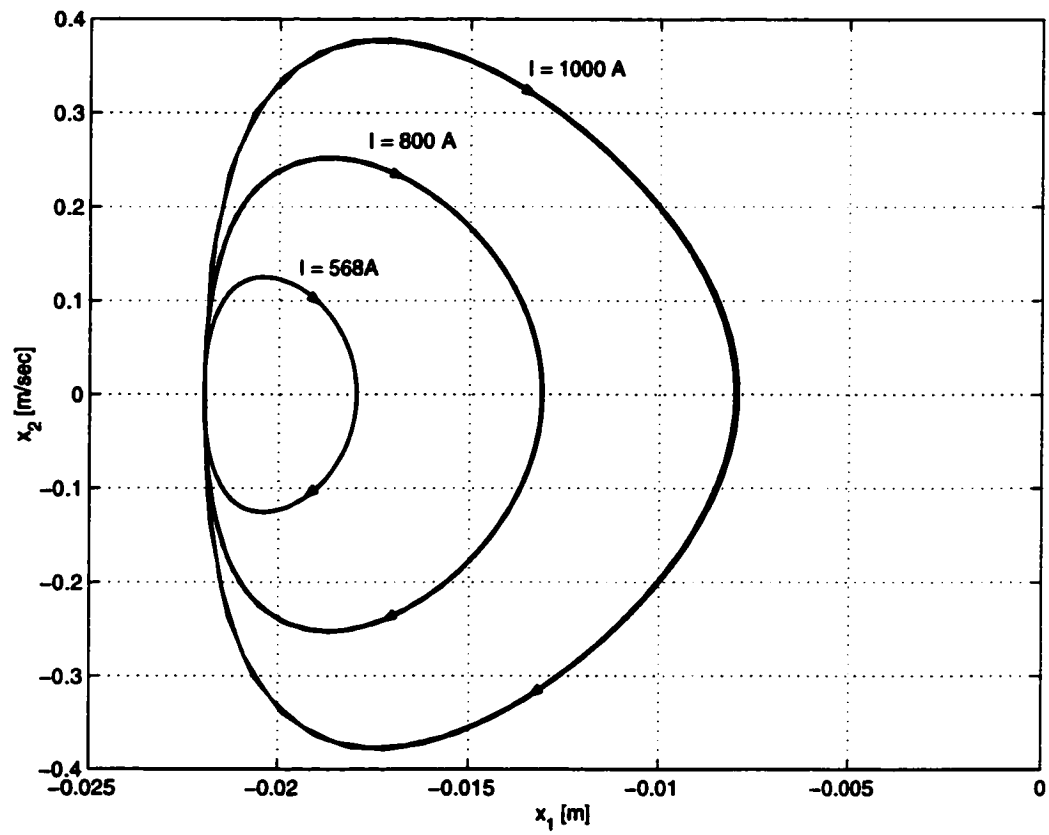
Figure 4.7: The phase trajectories for the different coil currents.
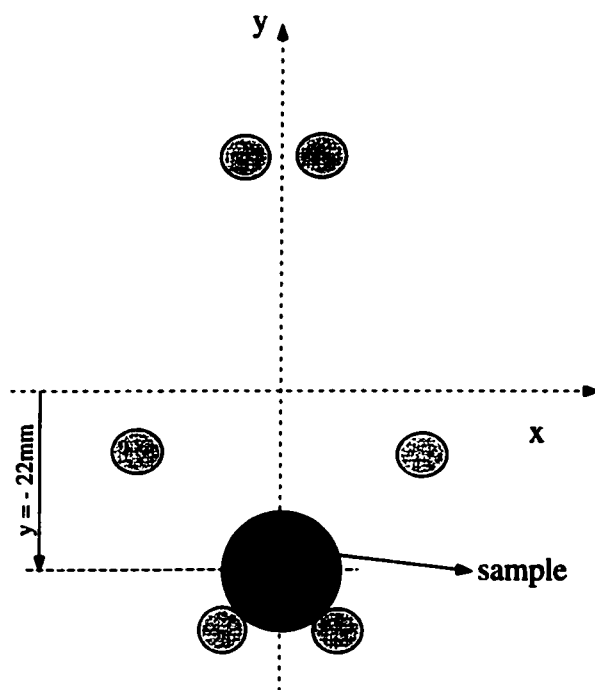
Figure 4.8: Initial condition of the sample in the levitator.
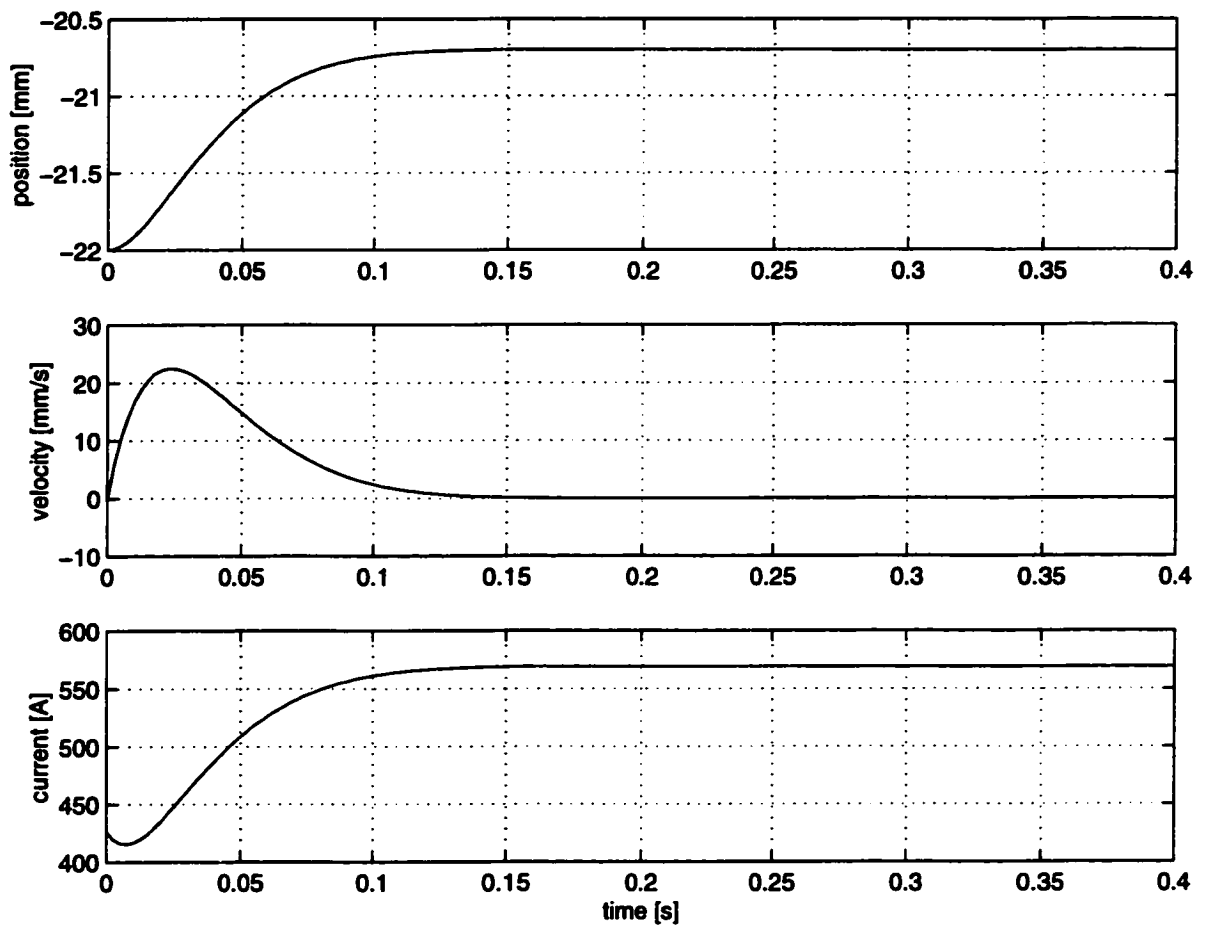
Figure 4.9: Pole placement control for x_{eq}= -20.7mm.

Figure 4.10: Pole placement control for the larger values of the levitation position.

Chapter 5

Conclusions

Containerless processing is important both for measurements of the thermophysical properties of metals and for producing very pure and homogeneous melt in material processing. However, it has been difficult to maintain the stability of the levitated sample inside the levitator.

Recently, Bayazitoglu and Shampine developed the longitudinal electromagnetic levitator, which has some unique advantages such as the ability to provide a 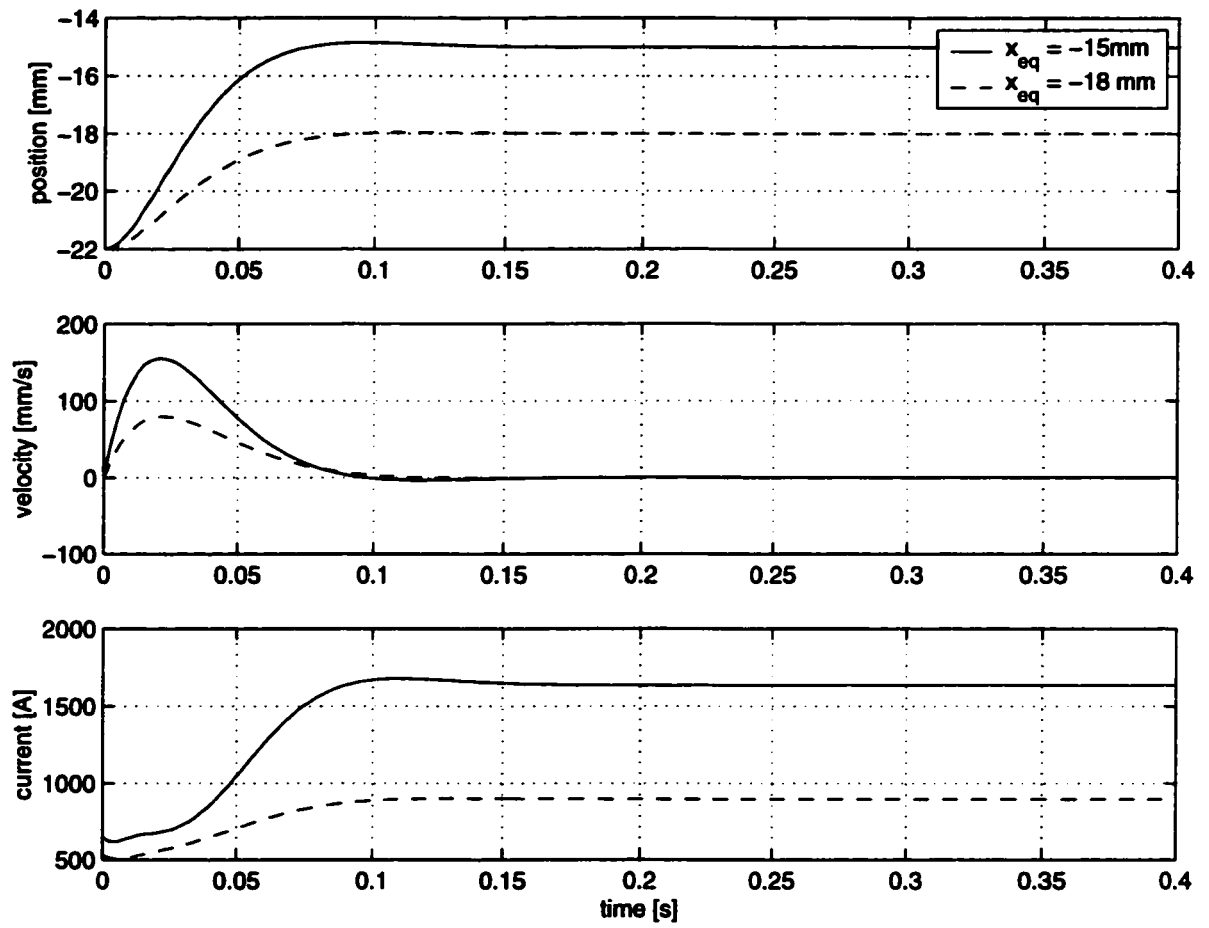strong levitation force and to minimize the tendency of the sample to rotate and vibrate. But, they also found that the sample must be initially released very near at its equilibrium or subtantial sample vibrations will be experienced.

Previous studies done in the longitudinal levitator have concluded that the oscillations of the sample constitute the major practical problem in applying this process accurately. If one had a dynamical model, it would become possible to design a feedback control for the stability of the sample.

The main contribution of this thesis is to present a dynamical model of the levitated sample to address this need. The dynamical effect of the sample's motion was considered for the first time to characterize the levitation force acting on the sample. Based on this analysis, the damping component of the levitation force was analytically derived. It was found that the sample's motion in the levitator produces a non-linear damping effect, which is a function of the system parameters such as coil current, current frequency, coil configuration and the diameter of the sample.

The influences of the system parameters on both the lifting and the damping components of the levitation force were separately illustrated to provide a framework for future works. The coil current, which determines the levitation position and the lifting capacity, had the strongest influence on both the lifting and the damping force. At low frequencies, the current frequency had a considerable effect on the lifting force. However, the lifting force reached an asymptotic value at high frequencies.

The lifting force also increased as the electrical conductivity increased at low frequencies. But, the influence of the electrical conductivity on the lifting force dissappeared at high frequencies. For non-ferromagnetic materials, only the electrical conductivity depends on temperature. Therefore it can be concluded that the lifting force is independent of the temperature of the sample at sufficiently high frequencies.

As the results of the dynamical analysis showed, the sample's motion inside the levitator was affected by the initial position of the sample, coil currrent and the coil configuration. Several simulations were performed to illustrate these effects on the sample's dynamics. Even a very small deviation from the equilibrium caused substantial oscillations of the sample as experimentally found in [7, 38]. The result of the dynamical analysis also showed that the magnitude of the damping force is relatively small but not eligible when compared with the lifting force.

It was also shown that it is possible to obtain a stable levitation by an appropriately designed feedback control strategy. Assuming that all state variables are available for feedback, two feedback control technique were applied to achieve stable levitation. In PD based control, the feedback gains were selected by trial and error for an equilibrium position, and the sample oscillations were eliminated within 0.4 seconds. But the selected gains could not provide the same performance for different levitation positions.

To improve the performance of the control system, the pole-placement technique was implemented. The effectiveness of this technique has been verified with several simulations for different levitation position. It can be concluded that this technique can be effectively used for the stabilization of the longitudinal levitation process.

Future Work

As a future work, it is possible to implement the control strategy introduced in this study in order to build a computer controlled levitation system. A possible configuration could include:

- **RF Power Source** with adjustable output current by external control signal.

- **Personel Computer** with control code implemented.

- **Data Acquisition (DAQ) Board** with analog input and analog output channels.

- **Electro-optical Displacement Transducer** with analog output.

Figure 5.1 shows the components and the signal flow of the system. During the levitation process, the position of the sample is measured by an electro-optical displacement transducer, which is based on the measurement of the intensity of the reflected light from the target. The tranducer has a light sensor source sending the light to the moving target sample and a light sensor receiving the light [20]. Typically, infrared light emitting diodes (LED's) or photosensitive diodes are used in this transducer. The velocity of the sample is obtained from the time derivation of the position signal.

Data acquisition board receives the analog position signal and converts it to the digital signal to be evaluated by the control code. Also, DAQ board sends the control signal to the RF Power Source. The control signal is produced by the developed

control strategy, which is basically a software code installed on the computer. In the system, the computer can also be used to monitor the system variables such as position, velocity and the current. Finally, RF Power Source produces the high frequency controller current for the longitudinal levitator.
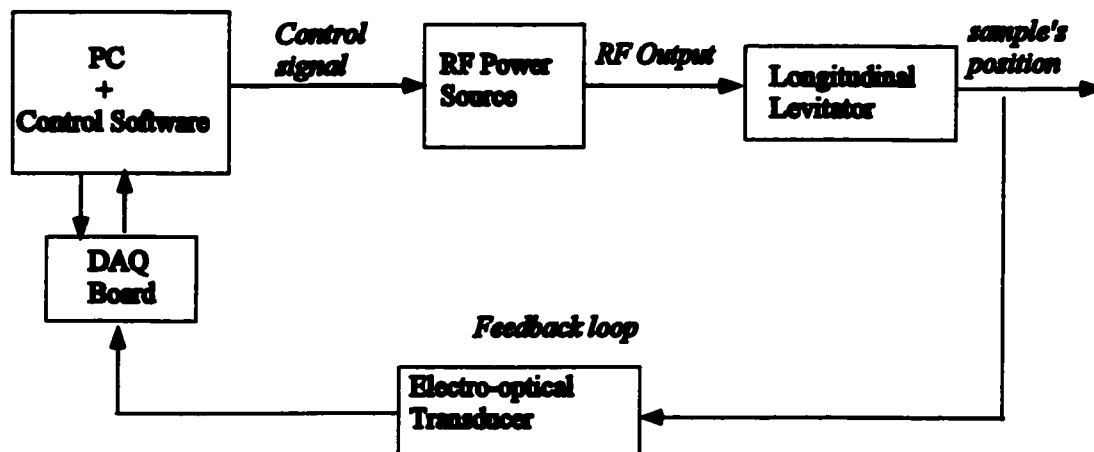
Figure 5.1: The schematic drawing of the computer controlled longitudinal levitation system

Appendix A

Lifting Force Derivation

The miscellaneous integral formulas of Bessel Function:

$$\int_0^x J_m(\alpha x)J_m(\beta x)x\,dx =$$

$$\frac{x}{\alpha^2 - \beta^2}[\alpha J_m(\beta x)J_{m+1}(\alpha x) - \beta J_m(\alpha x)J_{m+1}(\beta x)] \qquad (A.1)$$

where $\alpha^2 - \beta^2$ is not equal to zero. Therefore, we can obtain

$$
\begin{aligned}
Q_n &= \int_0^a J_n(k_1 a)J_n(k_1^* r)r\,dr \\
&= \frac{a}{2k_1}[J_n(k_1^* a)J_{n+1}(k_1 a) - iJ_n(k_1 a)J_{n+1}(k_1^* a)] \\
&= \frac{a}{2k_1}[-J_{n-1}(k_1 a)J_n(k_1^* a) + iJ_{n-1}(k_1^* a)J_n(k_1 a)] \qquad (A.2)
\end{aligned}
$$

and

$$Q_{n+1} = \frac{a}{2k_1}[-J_n(k_1 a)J_{n+1}(k_1^* a) + iJ_n(k_1^* a)J_{n+1}(k_1 a)] \qquad (A.3)$$

as given in [38]. Thus, the lifting force becomes

$$F_l = \frac{\pi \mid k_1 \mid^2}{2\mu_0} \sum_{-\infty}^{\infty} C_n C_{n+1}^* J_n(k_1^* a)J_{n+1}(k_1 a) \qquad (A.4)$$

By substituting Equation (2.21) and Equation (2.22) into the equation above and reaaranging the terms

$$F_l = \pi a\mu_0 \sum_{n=1}^{\infty}[\sum_{m=1}^{p}(\frac{a}{b_m})^{n-1}J_{n,m} \sum_{m=1}^{p}(\frac{a}{b_m})^{n}J_{n+1,m}^* Re(\frac{J_{n+1}(k_1 a)}{J_{n-1}(k_1 a)})] \qquad (A.5)$$

where $J_{n,m}$, which is the Fourier series of the surface currents on cylinder $r = b_m$, is given by [24]

$$J_{n,m} = \frac{\hat{I}_m}{2\pi b_m} e^{-jn\alpha_m} \tag{A.6}$$

and we know that

$$b_m e^{i\alpha_m} = c_m - w \tag{A.7}$$

or

$$b_m^n e^{in\alpha_m} = (c_m - w)^n \tag{A.8}$$

Assuming that the sample is located along the centerline of the levitator ($x = 0$ and $w = iy$), the time-averaged lifting force per unit length in the vertical direction becomes

$$F_{ly} = Im\{\frac{\mu_0 \hat{I}_m^2}{4\pi a} \sum_{n=1}^{\infty} [\{\sum_{m=1}^{p} (\frac{a}{c_m - iy})^n\}\{\sum_{m=1}^{p} (\frac{a}{c_m^* + iy})^{n+1}\} Re \frac{J_{n+1}(k_1 a)}{J_{n-1}(k_1 a)}]\} \tag{A.9}$$

Note that the time averaged lifting force is the imaginary part of the force formula given in [32, 39].

Bibliography

[1] Y. Bayazitoglu. Property determination at high temperatures by using electromagnetic levitation. In *Proc. of ITEC95*, volume 1, pages 12–20, Agadir, Morocco, 1995.

[2] Y. Bayazitoglu. Containerless processing by acoustic and electromagnetic levitation. In *Proceedings of the 11th IHTC*, volume 1, pages 23–28, August 1998.

[3] Y. Bayazitoglu and R. Shampine. Longitudinal electomagnetic levitator. *J.of Materials Processing and Manufacturing Science*, 5:79–91, July 1996.

[4] Y. Bayazitoglu and R.W. Shampine. Longitudinal electromagnetic levitator. U.S. Patent No. 5887018.

[5] Y. Bayazitoglu and P.V.R. Suryanarayana. Dynamics of oscillating viscous droplets immersed in viscous media. *Acta Mechanica*, 95:167–183, 1992.

[6] Y. Bayazitoglu, P.V.R. Suryanarayana, and U.B. Sathuvalli. High temperature thermal diffusivity determination procedure for solids and liquids. *AIAA J. Thermophysics*, 4(462-468), 1990.

[7] Y. Bayazitoglu and F.M. Young. 2-pole longitudinal electromagnetic levitators for use in containerless manufacturing. In *Proceeedings of 2000 IMECE*, Orlando, Florida, 2000.

[8] T. Baykara, R.H. Hauge, N. Norem, P.Lee, and J.L. Margrave. A review of containerless thermopysical property measurements and for liquid metals and alloys. *High Temperature Science*, 32, 1991.

[9] M. Bonvalot, P. Courtois, P. Gillon, and R. Tournier. Magnetic levitation stabilized by eddy currents. *Journal of Magnetism and Magnetic Materials*, 151:283–289, 1995.

[10] D. Dooling. Web Site. NASA Marshall Space Flight Center.

[11] E.C.Okress, D.M. Wroughton, and P.H.Brace J.C.R. Kely. Electromagnetic levitation of solid molten metals. *J. App. Phys.*, 23(545-552), 1952.

[12] I. Egry, G. Lohofer, P. Neuhaus, and S. Sauerland. Surface tension measurements of liquid metals using levitation microgravity, and image processing. *Int. J. Thermophysics*, 13:65–74, 1992.

[13] M.T. Enokizono and T. Yokoji. Experiment and analysis of levitation-melting method of induction furnace. *IEEE Transactions on Magnetics*, 31(6), November 1995.

[14] E.S.Bocian and F.J. Young. Some stability considerations in levitating melting. *J. Electrochem. Soc.:Solid State Science*, 118(2021-2026), 1971.

[15] E. Fromm and H. Jehn. Electromagnetics forces and power absorption in axially symmetric systems. *Brit. J. App. Phys.*, 16(653-663), 1965.

[16] F. Ghorbel and J. Dabney. A spherical pendulum system to teach key concepts in kinematics, dynamics, control, and simulation. *IEEE Transactions on Education*, 42(4), 1999.

[17] L.M. Holmes. Stability of magnetic levitation. *J. App. Phys.*, 49:3102–3109, 1978.

[18] K. Hassan K. *Nonlinear Systems*. Prentice Hall, N.J., 1996.

[19] O. Katsuhiko. *Designing Linear Control Systems with MATLAB*. Prentice Hall, N.J., 1993.

[20] A. D. Khazan. *Transducers and Their Elements: design and application*. Prentice Hall, 1994.

[21] S. Krishnan, G.P. Hansen, R.H. Hauge, and J.L. Margrave. Observations on the dynamics of electromagnetically levitated liquid metals and alloys at elevated temperatures. *Metallurgical Transactions*, 19 A:1939–1943, August 1988.

[22] S. Krisnan, J.K.R. Weber, P.c. Nordine, R.A. Schiffman, R.H. Hauge, and J.L. Margrave. Spectral emissivities and optical properties of liquid silicon, aluminum, titanium, and niobium at 632.8nm. *Prop. of Liquid Metals*, 5, 1991.

[23] B.Q. Li. The magnetothermal phenomena in electromagnetic levitation process. *Int. J. Engng Sci.*, 31(2):201–220, 1993.

[24] L.S.Pigott and G.F. Nix. Electromagnetics levitation of a conducting cylinder. In *Proc IEE*, volume 113, pages 1229–1235, 1966.

[25] H. Minegawa, Y. Suzuki, and J. Kawataba. Control of levitation in electromagnetic levitators under micrrogravity. *Japanese J.of Appl. Phys.*, 35(12B):1714–1716, 1996.

[26] J. Murphy and Y. Bayazitoglu. Laser flash thermal diffusivity determination procedure for high temperature liquid metals. *Numerical Heat Transfer*, 22(Part A: Applications):109–120, 1992.

[27] W.A. Peifer. Levitation melting. *Journal of Metals*, pages 487–493, 1965.

[28] M. Przyborowski, Hibiya, M. Eguchi, and I. Egry. Surface tension measurement of molten silicon by the oscilloting drop method using electromagnetic levitation. *J. of Crystal Growth*, 151:60–65, 1995.

[29] T. Richardson and G. Lohofer. Contactless electrical conductivity measurements of electromagneticaly levitated metallic melts. *Int. J. of Thermophysics*, 24(4):1029–1039, 1999.

[30] P.R. Rony. The electromagnatic levitation melting of metals. In *Vacuum Metallurgical Conference*, pages 55–135, 1964.

[31] T. Saito, Y. Shiaishi, and Y. Sakuma. Density measurement of molten metals by levitation technique at temperatures between 1800 and 2200 °C. *Transactions Iron and Steel Institute of Japan*, 9:118, 1969.

[32] R. Shampine and Y. Bayazitoglu. Analysis of the longitudinal electromagnetic levitator. *IEEE Transaction of Magnetics*, 33(6):4427–4433, 1997.

[33] R.W. Shampine. *Experimental and Analytical Results for Longitudinal Electromagnetic Levitation*. PhD thesis, Rice University, 1997.

[34] H. Soda, A. Mclean, and W.A.Miller. Surface tension measurements of liquid copper droplets. *Trans. Japan Inst. Metallurgy*, (18(6)):445–454, 1977.

[35] W. R. Synthe. *Static and Dynamic Electricity*. McGraw-Hill, New York, 1939.

[36] M. Vidyasagar. *Nonlinear Systems Analysis*. Prentice Hall, N.J., 1993.

[37] S. Yoda, S. Okuda, and K. Ikegami. Levitation with rotation control. U.S. Patent No. 5155651.

[38] X. Zhong. *The Lorentz Force and Temperature Distribution in a Longitudinal Electromagnetically Levitated Sample*. PhD thesis, Rice University, 1999.

[39] X. Zhong and Y. Bayazitoglu. Electromagnetic field and lifting capacity for longitudinal electromagnetic levitator. *IEEE Transaction on Magnetics*, 36(5):3746–3754, 2000.